8-2019

Data Driven Quickest Detection in Networks and Its Applications in Spectrum Sensing

Yifan Wang
University of Tennessee, ywang79@vols.utk.edu

Data Driven Quickest Detection in Networks and Its Applications in Spectrum Sensing

A Dissertation Presented for the

Doctor of Philosophy

Degree

The University of Tennessee, Knoxville

Yifan Wang

August 2019

Acknowledgments

Firstly, I would like to express my sincere gratitude to my Ph.D. advisor Prof. Husheng Li, for his continuous support of my study and research, for his patience, motivation, and immense knowledge. His guidance helped me in all the time of research and writing of this dissertation. I could not have imagined having a better advisor and mentor for my Ph.D study.

Besides my advisor, I would like to thank the rest of my committee: Dr. Seddik M. Djouadi, Dr. Arun Padakandla, and Dr. Xueping Li, for their insightful comments and encouragement from various perspectives.

My sincere thanks also go to Prof. Lijun Qian, who provided me opportunities to visit their lab in PVAMU for three summers, and who gave me valuable opinions on my research and publications.

I thank my fellow labmates, Liang Li, Jingchao Bao, Yawen Fan, Zhiyang Zhang, Rukun Mao and Zhenghao Zhang for all the discussions on related topics and dissertation writing, and for all the fun we have had in the last 6 years.

Last but not the least, I would like to thank my Parents, Baili Zhu and Yong Wang for constantly supporting me throughout the process of completing this dissertation and my life in general.

Abstract

Cognitive radio is one of the enabling technologies considered for the next generation communication systems for many mission-critical applications. In modern cognitive ratio systems, the spectrum is becoming increasingly crowded and expensive; thus spectrum sensing becomes more important than ever before.

In this dissertation, the study is focused on data driven quickest detection applied to energy detection based spectrum sensing. Firstly, a framework that integrates quickest detection and belief propagation is applied to the cooperative spectrum sensing where the primary user (PU) activities are heterogeneous in the space and dynamic in the time. The performance of the proposed scheme is analyzed mathematically. Using numerical simulations, detection performance measured by false alarm rate and average detection delay is obtained for different setups. Numerical simulations have demonstrated the validity of the proposed technique.

Secondly, we propose a universal quickest change detection scheme based on density ratio estimation for spectrum sensing by detecting the sudden change of spectrum (e.g., the emergence of PU), where neither the pre-change nor post-change distribution (even the distribution forms) is known to secondary users (SUs), thus achieving robustness to complex spectrum environment, where SUs have no prior information about the measurement distributions. The validity of the proposed schemes has been shown by numerical simulations.

Finally, we extend the detection of change in spectrum to millimeter-wave environment. As millimeter-wave is becoming part of the physical layer standard in the next-generation cellular network, it also brings about many questions and challenges. Not all the existing theories and methods for traditional wireless communication can apply directly to millimeter-wave communication because of the adoption of directional antenna and the high frequency

band used. We propose a data-driven spectrum change sensing technique based on mean recurrence time to efficiently detect the PU activities which is tolerant of small fluctuations. The proposed spectrum sensing works well without a priori knowledge of the sensed signal, and doesn't take assumption of independent and identically distributed random variables. It can also serve as a general framework for detection in other areas. The experimental results validate the proposed detection framework.

Table of Contents

List of Tables

List of Figures

Chapter 1

Introduction

The problem of detecting abrupt changes in the behavior of an observed signal or time series have been widely studied in various fields in recent decades [32]. The best solution to this problem, also known as quickest detection, aims at achieving minimum delay with as few false alarms as possible.

Cumulative sum (CUSUM) test is one of the most well known quickest detection methods, widely adopted in solving quality control, anomaly detection and many other change detection problems, among which, spectrum sensing is an important and intriguing one where change in spectrum occupancy needs to be monitored by wireless nodes and change be detected in a quickest manner.

Spectrum sensing is one of the key techniques, as well as design goals in cognitive radio (CR) systems, which has substantial impact on the applicability of cognitive radio in the future. As wireless communication technology advances, the spectrum is becoming increasingly crowded and expensive. By spectrum sensing this valuable resource can be more efficiently utilized. Generally speaking, spectrum sensing is to detect spectrum activities, such that secondary users (SUs) without license to the frequency band (which is licensed to primary users (PUs)) can then be able to communicate with each other in this band, when PUs are not present. In other words, SUs should be agile and have robust awareness of the presence or absence of PUs with acceptable detection delay and false alarm rate.

Despite the optimal performance CUSUM algorithm can achieve, there are several limitations when applying to actual scenarios like spectrum sensing in cognitive ratio network:

- Detection is single-point, which does not incorporate information shared by neighbors to improve accuracy.
- It usually requires prior knowledge of pre and/or post-change distribution.
- CUSUM test can only be applied to i.i.d. samples.

To the author's best knowledge, most of the work done in quickest detection either assumes known or partially known distributions, or have simple binary status change detection. The proposed methods extend quickest detection to broader application, combined and improved with other tools and algorithms, such as belief propagation (BP) and data-driven non-parametric sequential detection.

In this multi-part dissertation, I focused on the data driven quickest detection, applied in spectrum sensing. Firstly, in chapter **??** belief propagation combined with methodology inspired by CUSUM allows cooperative spectrum sensing with quickest detection. In chapter **??**, a universal data-driven quickest detection approach is proposed to empower the change detection without knowledge of pre and post change distribution. Finally, a universal detection framework is proposed in chapter 4 for change detection on non i.i.d. sequence, which can be applied to mmWave Spectrum sensing problem considering the special characteristics of wireless signal in mmWave network.

Part I

Coorperative Quickest Detection

Chapter 2

Belief Propagation and Quickest Detection Based Cooperative Spectrum Sensing in Heterogeneous and Dynamic Environments

This chapter is revised based on a journal paper published by Yifan Wang, Dr. Husheng Li and Dr. Lijun Qian:

Wang, Y., Li, H., & Qian, L. (2017). Belief propagation and quickest detection-based cooperative spectrum sensing in heterogeneous and dynamic environments. *IEEE Transactions on Wireless Communications*, 16(11), 7446-7459.

My primary contributions to this paper include formulation and modeling of the problem, identification of the research areas and objectives, design and conducting of the simulation experiments, theoretical analysis of the performance of proposed algorithm, and most of the writing.

Abstract

Cognitive radio is one of the enabling technologies considered for the next generation communication systems for many mission-critical applications. In cognitive radio systems, cooperative spectrum sensing is one of the key techniques that can improve the reliability and agility. In this chapter, a framework that integrates quickest detection and belief propagation is applied to the cooperative spectrum sensing where the primary user activities are heterogeneous in the space and dynamic in the time. The performance of the proposed scheme is analyzed mathematically. Using numerical simulations, detection performance measured by false alarm rate and average detection delay is obtained for different setups. The results show that the proposed scheme achieves better receiver operational curves than traditional detection method.

2.1 Introduction

Cognitive radio, based on software-defined radio, is considered as the next generation radio for many mission-critical applications, such as in the Joint Tactical Radio System (JTRS) program [26] and the DARPA xG program [7]. In cognitive radio systems, one of the key techniques, as well as design goals, is spectrum sensing, which has substantial impact on the applicability of cognitive radio in the future. As wireless communication technology

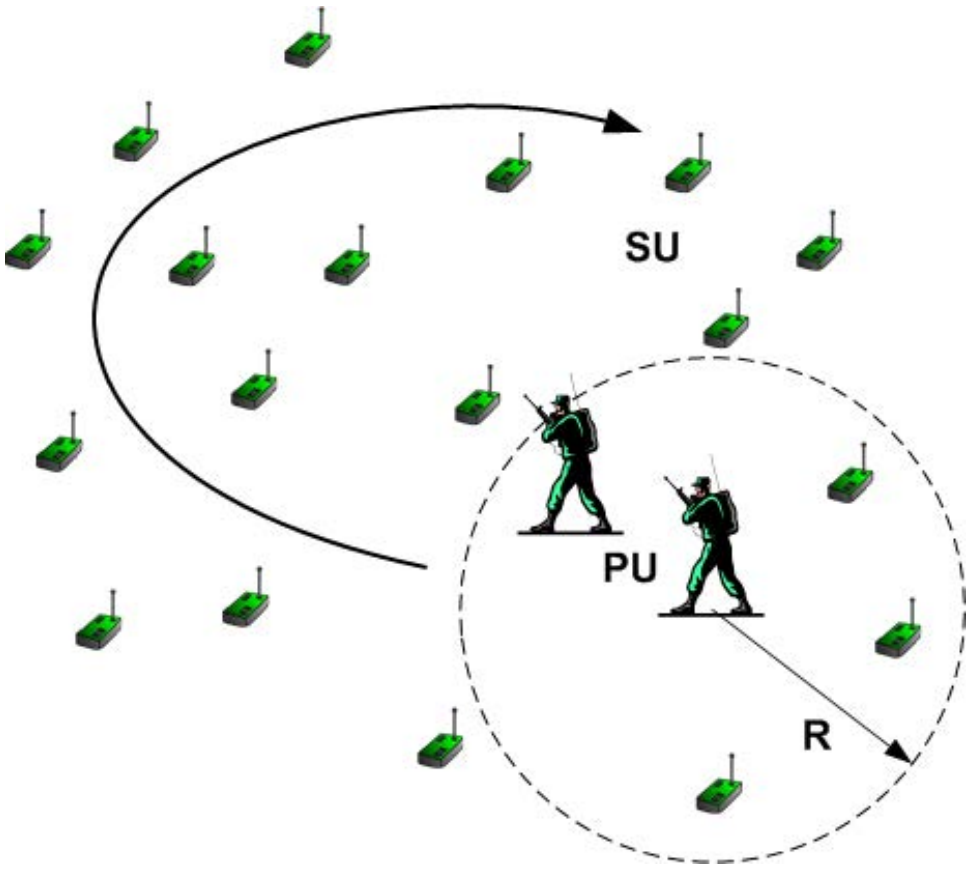

Figure 2.1: Moving primary users (soldier radios) and stationary secondary users (wireless sensor nodes) coexist in the battlefield.

advances, the spectrum is becoming increasingly crowded and expensive. By spectrum sensing this valuable resource can be more efficiently utilized. Generally speaking, spectrum sensing is to detect spectrum activities, such that secondary users (SUs) without license to the frequency band (which is licensed to primary users (PUs)) can then be able to use this band to communicate with each other when PUs are not present. In other words, SU should be agile and have robust awareness of the presence or absence of PUs with acceptable delay and detection error rate.

However, a single SU may not achieve a satisfying performance by itself because of channel fading and noise. When using cooperative spectrum sensing [4] [5] [6] [23] [39], SUs share their knowledge of spectrum status (PUs' presence) with neighbors, which has been proved to achieve lower error rate.

As a motivating example, consider the scenario shown in Fig. 2.1. The soldiers have priority in their communications and they are considered as PUs. The SUs are the sensors with cognitive radios that are deployed to monitor the battlefield. The PUs and SUs share the same frequency bands. The sensors are stationary while the soldiers may be mobile for carrying out a task. In this case, the sensors need to perform cooperative spectrum sensing accurately to avoid interfering the communications among the soldiers, and thus use the spectrum opportunistically and efficiently. Note that the spectrum situation could be different at different locations (thus being heterogeneous in the space) and at different times (thus being dynamic in the time).

In this chapter, we apply a powerful algorithm for statistical inference, namely belief propagation (BP) [3] [12], to achieve cooperative sensing. BP is an iterative message passing algorithm, which operates on a factor graph allowing marginal distributions to be computed efficiently. Information that is based on observation at each SU is propagated within the network; and each SU combines local observations with messages passed from its neighbors and compatibility information to compute the belief. The compatibility information is used because SUs are spatially close to each other and have certain correlation. However, the computation and communication overhead will be tremendous if SUs pass all the observations to all SUs within communication range and if all correlations among SUs are to be considered. Thereby in the BP framework [46] [47] [16] [17] [19] we adopt the Markov random field model to simplify the problem.

For cases of location fixed SUs and PUs, beliefs in SUs can usually converge. However, we are considering dynamic spectrum environment in this chapter, which does not allow the SUs to wait for the convergence of BP. Hence in order to quickly detect the change in spectrum activities, we incorporate the technique of quickest detection [32] [18] [20] [27] to identify the change. Essentially quickest detection exploits the history information by taking into consideration the recent data instead of only using those from current time. By doing so, even the slightest change can be accumulated, magnified and detected. We will apply a variant of the well-known cumulative sum (CUSUM) test to the BP framework. To our best knowledge, this is the first study integrating BP and quickest detection for the task of detecting changes in spatially heterogeneous and time dynamic environments. Our numerical result shows

that, by integrating quickest detection, the cooperative spectrum sensing can achieve better performance in terms of delay and false alarm rate than traditional approaches [16] without quickest detection integrated. We will also provide theoretical performance analysis for the quickest detection and BP in the context of cooperative spectrum sensing, with simplified setups.

The remainder of the chapter is organized as follows. The system model is introduced in Section 2.2. The BP framework in spectrum sensing is introduced in Section 2.3. In Section 2.4, the CUSUM algorithm for quickest detection is briefly discussed and its variant that fits in our application scenario is proposed. Section 2.5 gives the performance analysis for collaborative quickest detection and the convergence of BP subject to message passing error. Numerical results are provided in Section 2.6, and finally Section 2.7 draws the conclusion.

2.2 System Model

In this section, we introduce the physical model of the cognitive radio system and its abstract model using graphical models.

2.2.1 Physical Models

In this chapter, we assume that SUs are randomly and statically distributed in an area, in which PUs may emerge randomly (both in time and space). For simplicity, we consider a single communication channel in the spectrum, which is shared by SUs and PUs. We define the PU interruption range as a distance R within which the SUs should keep silent once any PU is active (otherwise it will cause significant interference to the PU). Therefore for SU i, its goal is to monitor the frequency band licensed to PUs and run the following hypothesis test:

$$\begin{cases} H_0 : X_i \leq X_{edge} \\ H_1 : X_i > X_{edge} \end{cases} \tag{2.1}$$

where X_i is the true received power at SU i from the PU, and X_{edge} is the expected power received when SU i is on the edge of the PU interruption range. Intuitively, H_0 is true when the received power at SU i is smaller than X_{edge}, and H_1 is true when it is larger than

that. The decision for an SU whether to quit or begin communication is made based on the outcome of the hypothesis test.

We make the following assumptions: 1) Not all SUs can communicate with each other; to do so one must be within a certain distance (denoted by D) of another, and each SU knows the distance to its neighbors to which it can talk. 2) SUs exchange information via a dedicated common control channel other than the data communication channel licensed to PU. 3) The observation Y_i (in dB scale) is Gaussian distributed $\mathcal{N}(X_i, \sigma_n^2)$, where σ_n^2 is noise power in dB scale and X_i is also in dB scale. 4) The a priori distribution of X_i is also Gaussian $\mathcal{N}(\mu_0, \sigma_0^2)$. The second and third assumptions are made to facilitate the BP framework, which simplifies the problem to a great extent and proves to incur negligible loss in performance [39]. As for the last one, the true value of prior probability may not be Gaussian and could be time-varying in practical case. We choose Gaussian prior to facilitate BP.

2.2.2 Abstract MRF Model

As one of the most well-known probabilistic graphical models, Markov random field (MRF) [2] is widely used to model systems in machine learning or social networks. Similarly to any other probabilistic models, the key to solving problems is to know the interdependencies among different variables. In our case, SUs that are close to each other have certain correlations on the power measurements and underlying statistics, which are actually complicated. To facilitate the BP procedure, we model our BP framework over an MRF. In the MRF, two non-adjacent random variables (corresponding to two non-adjacent SUs) are independent of each other given their neighboring variables. These variables satisfy pairwise Markov property. If we denote by N_i and N_j the two non-adjacent nodes in graph $G(V, E), (i, j) \notin E$, then $N_i \perp\!\!\!\perp N_j | N_{V\setminus\{i,j\}}$, where V, E are respectively vertices set and edges set in graph G and (i, j) stands for an edge that connects vertex i and j, $V\setminus\{i, j\}$ represents the vertices subset excluding i and j. $N_i \perp\!\!\!\perp N_j$ means they are independent.

We denote by $Z_i \in \{0, 1\}$ the spectrum occupancy detected by SU i, along with the two random variables defined in the previous section, X_i and Y_i, which are the true received power and the observation of received power, respectively. Note that here Y_i is a version

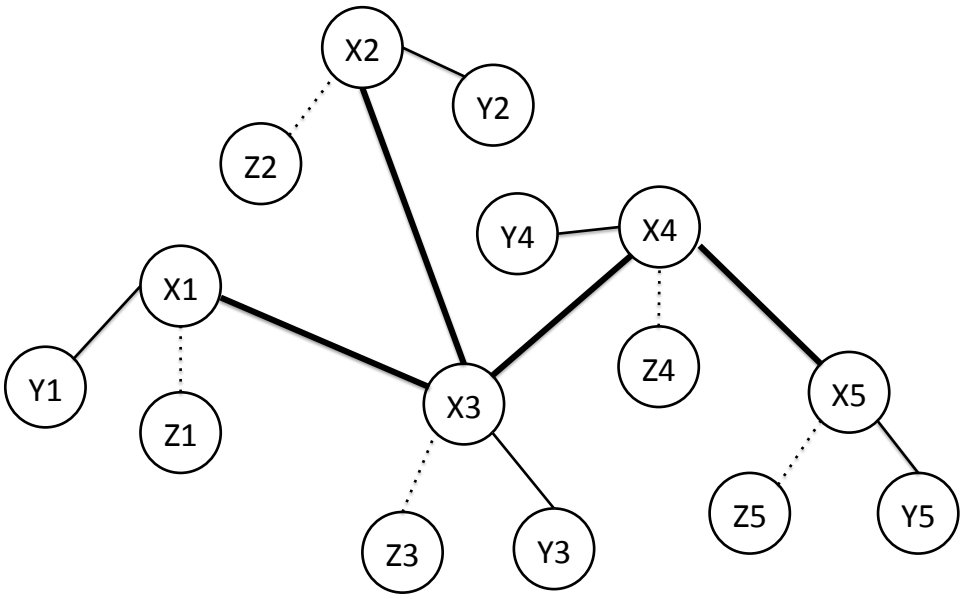

Figure 2.2: A Markov random field with five nodes each with three random variables: X, Y and Z.

of X_i, corrupted by noise and fading. As we discussed above, Y_i and Y_j are independent of each other if SU i and j are not adjacent in the cognitive radio network. As illustrated in Fig. 2.2, for example, Y_1 and Y_4 are independent.

2.3 BP For Cooperative Sensing

In this section, we will derive the BP framework for cooperative spectrum sensing. There have been some studies using BP in cooperative spectrum sensing. Fusion center is used in [47] to collect data from SUs, and imperfect communication channel for BP is considered. [16] proposed the BP framework for a system where SUs may have different decisions on whether to transmit or not based on observed signal over the target spectrum and thus the spectrum sensing can be done only in a distributed manner. In [17], the SUs conduct the BP based spectrum sensing by completing the entries of channel state matrix which represents channel states at different locations. And in [35], cooperative spectrum sensing subject to dynamic primary users' activities are discussed but limited to ON-OFF state changes. To

our best knowledge, there have been no previous studies on cooperative spectrum sensing where the primary user state is represented by some multi-value variables like power level, rather than just binary states of ON and OFF.

We adopt the MRF model which is also used in [16], as it can be represented as a factor graph over which BP is carried out. Based on the MRF model and the assumption that all the SUs satisfy the pairwise Markov property, the joint probability of $\boldsymbol{X}$ given observations $\boldsymbol{Y}$, where $\boldsymbol{X} = (X_1, X_2, ..., X_N), \boldsymbol{Y} = (Y_1, Y_2, ..., Y_N)$ can be represented in a factorization form:

$$P(\boldsymbol{X}|\boldsymbol{Y}) = \prod_{i=1}^{N} \psi_i(X_i|Y_i) \prod_{i \neq j} \psi_{ij}(X_i, X_j|Y_i, Y_j), \tag{2.2}$$

where ψ_i is called the local function, and ψ_{ij} is called the compatibility function representing the correlation of two neighboring SUs, as defined in section III of [16],

$$\psi_{ij}(X_i, X_j) = C \exp\left(\frac{\rho_{ij}(X_i - \mu_0)(X_j - \mu_0)}{\sigma_0^2}\right) \tag{2.3}$$

where C is a constant and ρ_{ij} is a function of d_{ij}, distance between i and j. Our goal is to compute the marginal probability $P(X_i|Y_1, Y_2, ..., Y_N)$ for SU i such that SU i can have a correct result from hypothesis test 4.1.

2.3.1 Belief Propagation

We first assume that the spectrum is stationary; i.e., the PU does not move and keeps its transmission status. Then, BP is carried out with a fixed number of iterations before decisions are made. To estimate the spectrum occupancy Z_i on each SU, we need to estimate X_i given $\mathbf{Y}$. Here $\mathbf{Y}$ is the observations corresponding to all $\mathbf{X}$. The local function can be initially computed as in (2.4) using a priori information and local observation Y, where the density of a priori distribution $f_X = \mathcal{N}(\mu_0, \sigma_0^2)$, and the conditional density $f_{Y|X} = \mathcal{N}(X, \sigma_n^2)$

$$f_{X|Y}(x|y) = \frac{f_{Y|X}(y|X=x) f_X(x)}{\int f_{Y|X}(y|X=x) f_X(x) dx} = K \cdot \exp\left[-\frac{(x - \frac{b}{2a})^2}{2 \cdot \frac{1}{2a}}\right]. \tag{2.4}$$

This is subject to a new Gaussian distribution $N(\mu, \sigma^2)$, where

$$\mu = \frac{b}{2a}, \sigma^2 = \frac{1}{2a}, a = \frac{1}{2\sigma_0^2} + \frac{1}{2\sigma_n^2}, b = \frac{\mu_0}{\sigma_0^2} + \frac{y}{\sigma_n^2} \ . \tag{2.5}$$

Algorithm 1: BP with fixed number of iterations

Input: Observation of received power level on each SU: $\mathbf{Y} = \{Y_1, Y_2, \ldots, Y_N\}$
Output: Spectrum occupancy detected by each SU: $\mathbf{Z} = \{Z_1, Z_2, \ldots, Z_N\}$

for $i \leftarrow 1$ ***to*** N **do**
  $a_i \leftarrow \frac{1}{2\sigma_0^2} + \frac{1}{2\sigma_n^2}$ $b_i \leftarrow \frac{\mu_0}{\sigma_0^2} + \frac{Y_i}{\sigma_n^2}$
  $\mu_i \leftarrow \frac{b_i}{2a_i}$ $\sigma_i^2 \leftarrow \frac{1}{2a_i}$
for $l \leftarrow 1$ ***to*** $IterNum$ **do**
  for $i \leftarrow 1$ ***to*** N **do**
    for $j \leftarrow 1$ ***to*** N **do**
      if $j \neq i$ ***and*** $d(i,j) < D$ **then**
        $a_{i\to j}^l \leftarrow \frac{1}{2\sigma_i^2}$
        $b_{i\to j}^l \leftarrow \frac{\mu_i}{\sigma_i^2}$
      for $k \leftarrow 1$ ***to*** N **do**
        if $k \neq i, j$ ***and*** $d(i,k) < D$ **then**
          $a_{i\to j}^l \leftarrow a_{i\to j}^l + \frac{1}{2\sigma^{2\,l-1}_{k\to i}}$ $\left(\sigma^{2\,0}_{k\to i}\right.$ initialized as $\left.+\infty\right)$
          $b_{i\to j}^l \leftarrow b_{i\to j}^l + \frac{\mu_{k\to i}^{l-1}}{\sigma^{2\,l-1}_{k\to i}}$ $\left(\mu_{k\to i}^0\right.$ initialized as $\left.\mu_0\right)$
      $(\mu_{i\to j}^l, \sigma^{2\,l}_{i\to j}) \leftarrow \mathcal{C}(a_{i\to j}^l, b_{i\to j}^l)$
for $i \leftarrow 1$ ***to*** N **do**
  $a_i \leftarrow \frac{1}{2\sigma_i^2} + \sum_j \frac{1}{2\sigma^2_{j\to i}}$ $b_i \leftarrow \frac{\mu_i}{\sigma_i^2} + \sum_j \frac{\mu_{j\to i}}{\sigma^2_{j\to i}}$
  $\mu_i \leftarrow \frac{b_i}{2a_i}$ $\sigma_i^2 \leftarrow \frac{1}{2a_i}$
  if $\dfrac{\mu_i - X_{edge}}{\sqrt{\sigma_i^2}} < Threshold$ **then**
    $Z_i \leftarrow 0$ $H_0^i \leftarrow true$
    else
      $Z_i \leftarrow 1$ $H_1^i \leftarrow true$
return $\boldsymbol{Z}$

Then we can consider the conditional density of X_i given neighbors' information. Here we assume that the neighbors of user i are not connected to each other, namely there is no loop in the factor graph $G(V, E)$. We will discuss the convergence of loopy BP in the performance analysis part. By the pairwise Markov property, Y_j ($\{i, j\} \in E$) are independent of each

other given X_i; therefore using the same manipulation as that in (2.4) we have the following equation:

$$\begin{aligned} f_{X_i|\mathbf{Y}}(x_i|\mathbf{y}) =& \frac{f_{\mathbf{Y}|X_i}(\mathbf{y}|X_i = x_i) f_{X_i}(x_i)}{\int f_{\mathbf{Y}|X_i}(\mathbf{y}|X_i = x_i) f_{X_i}(x_i) dx_i} \\ =& \frac{f_{X_i}(x_i) \prod_j f_{Y_j|X_i}(y_j|X_i = x_i)}{\int f_{X_i}(x_i) \prod_j f_{Y_j|X_i}(y_j|X_i = x_i) dx_i} \\ =& K' \cdot \exp\left[-\frac{(x_i - \frac{b_i}{2a_i})^2}{2 \cdot \frac{1}{2a_i}} \right], \end{aligned} \tag{2.6}$$

where

$$\begin{aligned} \mathbf{y} =& \{y_k | d(i,k) < D, 1 \le k \le N, k \ne i\} \\ a_i =& \frac{1}{2\sigma_0^2} + \frac{1}{2\sigma_n^2} + \sum_j \frac{1}{2\sigma_{j\to i}^2}, \\ b_i =& \frac{\mu_0}{\sigma_0^2} + \frac{y_i}{\sigma_n^2} + \sum_j \frac{\mu_{j\to i}}{\sigma_{j\to i}^2}. \end{aligned} \tag{2.7}$$

Here, ${\sigma^2}_{j\to i}$ and $\mu_{j\to i}$ are the two-number message sent from SU j to i, and in the beginning of the BP iteration, they are initialized as $+\infty$ and μ_0 respectively.

In order for SUs to send only useful messages, the belief passed from i to j should not include the one passed from j to i in the last round (as shown in line 11 to 13 Algorithm 1), thus yielding the intermediate messages from i to j as follows:

$$\begin{aligned} a_{i\to j} =& \frac{1}{2\sigma_0^2} + \frac{1}{2\sigma_n^2} + \sum_{k\ne i,j} \frac{1}{2\sigma_{k\to i}^2}, \\ b_{i\to j} =& \frac{\mu_0}{\sigma_0^2} + \frac{y_i}{\sigma_n^2} + \sum_{k\ne i,j} \frac{\mu_{k\to i}}{\sigma_{k\to i}^2}. \end{aligned} \tag{2.8}$$

However, in order to satisfy the MRF assumption, we have to take into account the compatibility function ψ_{ij} which represents the correlation of received powers at any two SUs, X_i and X_j. Thus after each iteration, we need to add in the compatibility function ψ_{ij} to compute a new pair of messages: $(\mu_{i\to j}, \sigma_{i\to j}^2) \leftarrow \mathcal{C}(a_{i\to j}, b_{i\to j})$. The detailed expression of

this function $\mathcal{C}$ is given in equation (14) and (15) in [16].

$$\begin{aligned}\mu_{i\to j} =& \frac{(e-f)\mu_0 + \frac{2f((e-f)\mu_0)+b_{i\to j}}{2(e+a_{i\to j})}}{e-\frac{f^2}{e+a_{i\to j}}} \\ {\sigma^2}_{i\to j} =& \frac{1}{2(e-\frac{f^2}{e+a_{i\to j}})}\end{aligned} \tag{2.9}$$

Hence after a fixed number of iterations, each SU will compute its own belief by a_i and b_i obtained in (2.7): $\mu_i = \frac{b_i}{2a_i}$ $\sigma_i^2 = \frac{1}{2a_i}$. Then decisions are made based on the normalized difference given in the line 18 of Algorithm 1, where X_{edge} is the average received power of an SU at the edge of primary user interruption range. If this difference is larger than the preset threshold, we believe that the hypothesis H_1 is true; otherwise H_0 is true.

It is shown in [16] that the fixed iterative BP achieves a better performance in terms of missed detection rate and false alarm rate when the iteration number increases, which is also more costly in the time. Yet, in practice, more and more applications require mobility for PU and SU. In the next subsection, we are going to discuss the situation in which a PU is moving among a group of fixed SUs and message passing suffers from communication loss.

2.3.2 Modified BP Algorithm for Dynamical Environment and Noisy Communications

The more realistic scenario in many mission-critical applications is that one or more PUs are moving in the area where SUs are deployed, for example, see Fig.2.1. In this situation, if the SU makes a decision every T iterations but using only the observations obtained before the BP begins, the information gathered for making decision will be obsolete (as shown in Algorithm 1), especially when the PU moves at a rather fast speed.

Based on this observation, it is required that each SU continuously update its local observation at every iteration (see Algorithm 2). However, the local function keeps changing with new information (observation at current time) continually introduced to the belief message that is to be passed out; this BP algorithm may never literally "converge" since each iteration runs with a new input. However, it is known that, in the case of Gaussian distribution, even loopy BP convergence is correct. [44].

In reality, BP in a wireless network is subject to communication error caused by channel loss and fading. When this happens, SU may choose to use belief information calculated in the previous iteration or to use a priori information to replace the otherwise successfully received message. The numerical result in section 2.6 shows that the performance of BP does not deteriorate sharply. And the convergence of loopy BP subject to communication error will be analyzed in the section 2.5.

Algorithm 2: BP with up-to-date local information

Input: Observation of received power level on each SU: $\mathbf{Y}^l = \{Y_1^l, Y_2^l, \ldots, Y_N^l\}$
Output: Spectrum occupancy detected by each SU: $\mathbf{Z}^l = \{Z_1^l, Z_2^l, \ldots, Z_N^l\}$

for $l \leftarrow 1$ ***to*** $RunningTime$ **do**
  for $i \leftarrow 1$ ***to*** N **do**
    $a_i \leftarrow \frac{1}{2\sigma_0^2} + \frac{1}{2\sigma_n^2}$ $b_i \leftarrow \frac{\mu_0}{\sigma_0^2} + \frac{Y_i^l}{\sigma_n^2}$
    $\mu_i \leftarrow \frac{b_i}{2a_i}$ $\sigma_i^2 \leftarrow \frac{1}{2a_i}$
  for $i \leftarrow 1$ ***to*** N **do**
    for $j \leftarrow 1$ ***to*** N **do**
      if $j \neq i$ ***and*** $d(i,j) < D$ **then**
        $a_{i\to j} \leftarrow \frac{1}{2\sigma_i^2}$
        $b_{i\to j} \leftarrow \frac{\mu_i}{\sigma_i^2}$
      for $k \leftarrow 1$ ***to*** N **do**
        if $k \neq i, j$ ***and*** $d(i,k) < D$ **then**
          $a_{i\to j} \leftarrow a_{i\to j} + \frac{1}{2\sigma_{k\to i}^2}$
          $b_{i\to j} \leftarrow b_{i\to j} + \frac{\mu_{k\to i}}{\sigma_{k\to i}^2}$
      $(\mu_{i\to j}, \sigma_{i\to j}^2) \leftarrow \mathcal{C}(a_{i\to j}, b_{i\to j})$
  for $i \leftarrow 1$ ***to*** N **do**
    $a_i \leftarrow \frac{1}{2\sigma_i^2} + \sum_j \frac{1}{2\sigma_{j\to i}^2}$ $b_i \leftarrow \frac{\mu_i}{\sigma_i^2} + \sum_j \frac{\mu_{j\to i}}{\sigma_{j\to i}^2}$
    $\mu_i \leftarrow \frac{b_i}{2a_i}$ $\sigma_i^2 \leftarrow \frac{1}{2a_i}$
    if $\frac{\mu_i - X_{edge}}{\sqrt{\sigma_i^2}} < Threshold$ **then**
      $Z_i^l \leftarrow 0$ $H_0^i \leftarrow true$
      else
        $Z_i^l \leftarrow 1$ $H_1^i \leftarrow true$
  return $\boldsymbol{Z}^l$

Note that in BP the belief passed from node i to j does not include the one passed from j to i in the last iteration. As a result, at time $l+1$ the i^{th} SU will forget its own observation

Y_i^l sampled at time l, because the message $(\mu_{i\to j}^l, {\sigma_{i\to j}^2}^l)$ sent to its neighbor j will not be included in the message $(\mu_{j\to i}^{l+1}, {\sigma_{j\to i}^2}^{l+1})$ sent back to i at time $l+1$. In addition, the local observation Y_i^l and Y_i^{l+1} are correlated, which indicates that the history information is lost during the BP procedure in this modified algorithm 2. In the next section, an algorithm of quickest detection that can well fit to our BP framework is introduced to tackle this issue.

2.4 Quickest Detection Within BP Framework

In this section, we embed the technique of quickest detection into the framework of BP, which enables both distributed and online sensing in the cognitive radio network.

2.4.1 CUSUM Test for Quickest Detection

In statistical analysis, quickest detection aims at identifying changes in the probability distribution of a stochastic process. Generally speaking, one needs to decide whether a change has occurred at a certain time. Cumulative sum (CUSUM) test is one of the widely used quickest detection methods, which is proved to achieve the optimal performance even in the non-asymptotic case[1] [24][20] . In CUSUM test, two hypotheses H_0 and H_1 are tested based on the observation sequence $\{B_i, i = 1, 2, 3, \dots\}$. We assume that the sensed signal power at SU is a sequence of independent and identically distributed (i.i.d.) random variables $\{B_i, i = 1, 2, 3, \dots\}$, that follows a certain distribution f_0 for $i < T_C$ and another distribution f_1 after that $i \geq T_C$, where T_C is the unknown change point to be detected.

Basically, CUSUM test tries to identify the change that occurs in a random process in the quickest manner. The CUSUM stopping time is defined as:

$$T^* = \inf\{t \geq 0 | S(t) \geq h\}, h \geq 1 \tag{2.10}$$

[1]The CUSUM stopping time is the stopping time that achieves the smallest possible detection delay for any given level of the expected time between false alarms.

where

$$\begin{aligned} S(t) &= \max_{1\le j\le t}\left\{\prod_{r=j}^{t} L(B_r)\right\} \\ &= \max\left\{\prod_{r=1}^{t} L(B_r), \prod_{r=2}^{t} L(B_r), \ldots, L(B_t)\right\} \\ &= \max\left\{S(t-1), 1\right\} \times L(B_t) \end{aligned} \tag{2.11}$$

where B_r is the observation at time r, and $L(B_r)$ is its likelihood ratio defined as

$$L(B_r) = \frac{df_1}{df_0}(B_r) \tag{2.12}$$

We can obtain a more convenient form for the CUSUM detection. Let

$$s(t) = \log S(t),\ l(t) = \log L(B_t),\ \gamma = \log h. \tag{2.13}$$

Then we can rewrite equations (2.10) and (2.11) as:

$$T^* = \inf\{t \ge 0 | s(t) \ge \gamma\}, \gamma \ge 0 \tag{2.14}$$

$$s(t) = \max_{1\le j\le t}\left\{\sum_{r=j}^{t} l(r)\right\} = \max\{s(t-1), 0\} + l(t) \tag{2.15}$$

Intuitively, the log-likelihood ratio (LLR) $l(t)$ has a negative mean under H_0 and then CUSUM remains around 0, whereas the LLR mean is positive under H_1, then making CUSUM drifting upwards until it crosses the threshold γ.

2.4.2 Quickest Detection Applied to BP Framework

In our BP framework, the hypotheses are not tested directly based on the local observations. Instead, an SU i acquires belief messages from its neighbors $(\mu_{j\to i}, \sigma^2_{j\to i})$, and then makes decision according to the newly computed belief (μ_i, σ_i^2) , which correspond to the moments of the conditional distribution of X_i given Y_j from neighbors. However, as is mentioned in the previous section, the SU cannot remember its past observation or past belief messages;

therefore we apply a quickest detection that utilizes history information to improve the system performance.

Note that in Eq. (2.15), $s(t)$ is the maximum of t summations; i.e,

$$s(t) = \max_{1 \le j \le t} \left\{ \sum_{r=j}^{t} l(r) \right\}. \tag{2.16}$$

Assume that the change is detected at time T^* by the CUSUM test. We can then confirm that at least one of these T^* products is greater than or equal to the threshold h, or intuitively, at least one of these products 'hits' the threshold. Equivalently, if we examine these T^* products and find any of them hitting the threshold, we can claim that a change has been detected.

Knowing that each product of likelihood ratios indicates the belief level of the alternative hypothesis H_1 (the larger it is, the more likely H_0 will be rejected), we can use the belief of SU_i, or equivalently $P(X_i^t | Y_i^j, Y_i^{j+1}, \ldots, Y_i^t, \overline{Y}_i^t)$ to approximate $\sum_{r=j}^{t} l(r)$, where $\overline{Y}_i^t$ are observations of all but SU i at time t. Then by (2.6) we have the following joint distribution for SUs i given the current and past $t-j$ observations at time t along with belief messages acquired from neighboring SUs:

$$\begin{aligned} f_{X_i^t|\mathbf{Y}^j}(x_i^t | \mathbf{y}_i^j, \overline{y}_i^t) =& K'' \cdot \exp\left[-\frac{(x-\mu_i^j)^2}{2\sigma_i^{2j}} \right] \\ =& K'' \cdot \exp\left[-\frac{(x-\frac{b_i^j}{2a_i^j})^2}{2 \cdot \frac{1}{2a_i^j}} \right] \end{aligned} \tag{2.17}$$

where

$$\begin{aligned}
\mathbf{y}_i^j =& \left\{y_i^j, y_i^{j+1}, \ldots, y_i^t\right\} \\
\overline{y}_i^t =& \left\{y_m^t | d(i,m) < D, 1 \le m \le N, m \ne i\right\} \\
a_i^j =& \frac{1}{2\sigma_0^2} + \frac{t-j+1}{2\sigma_n^2} + \sum_m \frac{1}{2\sigma_{m\to i}^2} \\
b_i^j =& \frac{\mu_0}{\sigma_0^2} + \sum_j^t \frac{y_i}{\sigma_n^2} + \sum_m \frac{\mu_{m\to i}}{\sigma_{m\to i}^2} \\
\mu_i^j =& \frac{b_i^j}{2a_i^j},\ \sigma_i^{2j} = \frac{1}{2a_i^j}
\end{aligned} \tag{2.18}$$

and K'' is a constant, similar to K' in equation (2.6).

The two numbers, μ_i^j and σ_i^{2j}, are the computed belief of SU i after the t^{th} iteration, which can be used to estimate $\sum_{r=j}^t l(r)$ in the CUSUM test (2.15). To fit this into BP framework, each SU has to store $t-j$ past samples and maintain $t-j+1$ belief messages that are to be sent to each of its neighbor. Considering the cost and the fact that correlation between observations sampled long time ago and the current ones is weak, we make a tradeoff between communication overhead and quickest detection performance by adopting only the recent L measurements. Specifically, we define

$$\begin{aligned}
T_i^* =& \inf\{t \ge 0 | s_i(t) \ge h\}, h \ge 0, \\
s_i(t) =& \max_{t-L+1 \le j \le t} \left\{ \frac{\mu_i^j - X_{edge}}{\sqrt{\sigma_i^{2j}}} \right\}
\end{aligned} \tag{2.19}$$

Note that there are two values for the threshold h: one is for detecting changes from H_0 to H_1, which is positive, while the other is negative, with the inequality sign reversed and min instead of max, for the detection of change from H_1 to H_0.

Thus the CUSUM algorithm can be well adapted to the BP framework. The algorithm procedure is almost the same as Algorithm 2 except for the following aspects:

- All SUs maintain a memory window of length L, where they store the most recent L local observations. Each SU keeps the previous hypothesis test result such that they know which change to detect (from H_0 to H_1 or from H_1 to H_0).

- Messages propagated between SUs include L different pairs of $(\mu^j_{m\to i}, \sigma^{2j}_{m\to i})$ according to Eq. (2.18).

- When making a decision, SUs take all the L computed beliefs into consideration. If the standardized difference of any of these believes hits the threshold h as in (2.19), the SU claims a change and takes the corresponding action.

2.5 Performance Analysis

In this section we will analyze the performance and convergence of BP in Gaussian Markov Random Field (GMRF), and cooperative quickest detection separately, since it is too complicated to analyze both jointly.

2.5.1 Convergence of BP Subject to Communication Errors

The convergence of BP has long been a difficult problem to tackle, especially in arbitrary graphs where various cycles exist. It is known to all that Pearl BP [29] is guaranteed to converge to the correct posterior probabilities for singly connected graph or a tree. A proof has been given in [44] that, in GMRF, BP converges with correct means, even when the graphical model is arbitrarily connected. When the BP procedure is subject to communication error or loss, it may have some impact on the result of BP. An SU may fail to send the message to some of its neighbors; therefore those that fail to receive the belief message cannot calculate and update the new message intended for their neighbors. However, as we proposed in Section 2.3, the node who does not correctly receive the belief message could instead use the previous incoming message for current calculation. We thereby give the analysis on convergence of BP that's subject to communication failure.

BP based cooperative spectrum sensing, as described in Section 2.3 of this chapter, can be modeled as message passed over Gaussian MRF. Each SU i is modeled to have two virtual nodes: the true received power level x_i and its observed version y_i corrupted by noise and fading. x_i is connected to x_j if user i and j can communicate with each other. y_i is only connected to the corresponding x_i.

In the GMRF, the joint distribution of $\boldsymbol{z} = \begin{pmatrix} \boldsymbol{x} \\ \boldsymbol{y} \end{pmatrix}$ can be written as:

$$P(z) = ae^{-\frac{1}{2}\boldsymbol{z}^T V \boldsymbol{z}}, \quad V = \begin{pmatrix} V_{xx} & V_{xy} \\ V_{yx} & V_{yy} \end{pmatrix}, \tag{2.20}$$

where V_{xy} and V_{yx} are diagonal matrices and $V_{xx}(i,j) = 0$ if user i and user j are not adjacent because of the property of GMRF, and a is a constant. The goal of our BP is to estimate the marginal probability of each x_i, or in the context of GMRF, to estimate the marginal posterior mean and variance of x_i , given observations y_i and belief messages passed from neighbors $x_j, j \in N(i)$, where $N(i)$ represents the collection of SUs that are graphically connected to SU i.

From Eq. (2.20), by marginalizing $\boldsymbol{x}$ and completing the square in the exponent we have

$$\begin{aligned} \boldsymbol{z}^T V \boldsymbol{z} =& \boldsymbol{x}^T V_{xx} \boldsymbol{x} + 2\boldsymbol{x}^T V_{xy} \boldsymbol{y} + \boldsymbol{y}^T V_{yy} \boldsymbol{y} \\ =& (\boldsymbol{x} - \boldsymbol{\mu})^T V_{xx} (\boldsymbol{x} - \boldsymbol{\mu}) + C \end{aligned} \tag{2.21}$$

$$\boldsymbol{\mu} = -V_{xx}^{-1} V_{xy} \boldsymbol{y} \qquad V_{xx} \boldsymbol{\mu} = -V_{xy} \boldsymbol{y} \tag{2.22}$$

where $\boldsymbol{\mu} = E[\boldsymbol{x}]$. And the covariance matrix $C_{\boldsymbol{x}|\boldsymbol{y}} = V_{xx}^{-1}$. We denote by $C_{x_i|\boldsymbol{y}}$ the i^{th} row of $C_{\boldsymbol{x}|\boldsymbol{y}}$, which represents the covariances between x_i and all other x. And it is easy to see that the marginal posterior variance of x_i, given observation $\boldsymbol{y}$, is $C_{x_i|\boldsymbol{y}}(i)$.

We all know that BP converges correctly in a tree which has no loops. Hence, to analyze the convergence of loopy BP, one can find a way to relate the loopy BP's structure to some structure that we are familiar with, namely a tree. To facilitate the following proof, all the deductions are illustrated by a simple graph given in Fig. 2.3a, where 5 SUs are passing belief message to each other. Note that the white nodes represent $\{x_i\}_i$ while the black ones represent corresponding observations $\{y_i\}_i$. For clarity, since y_i is only connected to x_i which has no influence of the whole BP procedure, it will not be shown in other figures of the chapter.

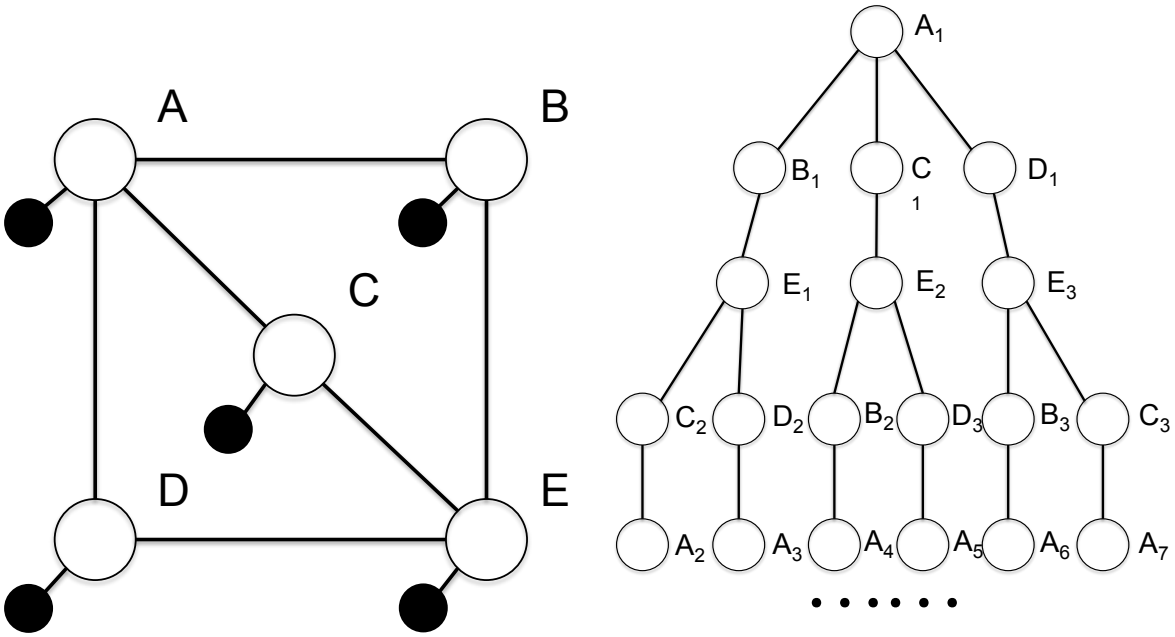

(a) A loopy Markov random field.

(b) An unwrapped tree $\hat{G}$ from node A.

Figure 2.3: In (a) nodes represented by white circles are x_i, nodes represented by black circles are y_i. In (b), only 4 iterations are shown

In order to compare the correct posterior and the loopy beliefs, we construct an unwrapped tree from the original graph with loops, as shown in Fig. 2.3b. We denote the original graph by G and unwrapped tree by $\hat{G}$. Basically we can expand the unwrapped tree from any node in G, to any depth in the following manner: 1) choose any node to be the root of $\hat{G}$. 2) find all its neighbors in the original graph as its children nodes. 3) for each of the nodes in Step 2 find the corresponding neighbors except for its parent node, as the children. 4) repeat Steps 2 and 3 till $\hat{G}$ has the required depth T.

In $\hat{G}$, information sent from the root node A goes down towards the leaves and arrives at any nodes of depth T after T iterations in G. Hence, $\hat{G}$ expanded from node A can be intuitively viewed as the information flow from A for T iterations. Or viewed from bottom the messages received by node A after T iterations in G are equivalent to the messages that will be received by root node A in $\hat{G}$.

The key relationship between G and $\hat{G}$ is that some statistics of replica nodes $A_i, B_i, C_i, \cdots (i = 1, 2, ...)$ in $\hat{G}$ are copies of those of $A, B, C, \cdots$ in G. Most importantly, we try to relate the inverse covariance matrix of G to $\hat{G}$. First we scan the unwrapped tree in

an order from root to leaves and from left to right, such that the leaf nodes are at the end of the scanned sequence. We index the sequence with natural number. Denote by $\hat{\boldsymbol{x}}$ the vector of values scanned in this way, and $\hat{\boldsymbol{y}}$ the observed version of $\hat{\boldsymbol{x}}$. With the above mentioned notation $\hat{\boldsymbol{x}}$ to represent vectors $\hat{G}$, all elements $\hat{V}_{xy}(i,j)$ and $\hat{y}_i$ are copies of $V_{xy}(I,J)$ and y_I, where $\hat{x}_i$ and $\hat{x}_j$ in $\hat{G}$ are replicas of x_I and x_J in G, and $\hat{V}_{xx}(i,j)$ for non-leaf nodes i and j is the copy of $V_{xx}(I,J)$. As for leaf nodes, it is not the case because leaf node $\hat{x}_i$ does not have the same complete neighbor set as non-leaf nodes do. Thus the statistics of leaf node $\hat{x}_i$ are different from those of non-leaf node $\hat{x}_j$ where $\hat{x}_i$ and $\hat{x}_j$ refer to the same node x_I in G.

When communication error or failure occurs during the belief message passing, a node should use the previous incoming message instead to update the belief. Then we construct a buffer node $\hat{x}_{i'}$ in the unwrapped tree $\hat{G}$ such that the failed message from $\hat{x}_i$ to $\hat{x}_j$ can be stored in this virtual node and sent to $\hat{x}_j$ at the next update. Thus we can modify $\hat{G}$ as shown in Fig. 2.4. For simplicity here we only show one error occurrence in this figure.

Then we use an $m \times n$ matrix Q as in Eq. (2.23) to map G to $\hat{G}'$, where m is the number of nodes in unwrapped tree $\hat{G}'$ and n in original cyclic graph G. Each row in Q stands for a node in $\hat{G}'$, and the rows are sorted in the breadth first order as in the unwrapped tree.

$$Q = \begin{bmatrix} 1 & 0 & 0 & 0 & 0 \\ 0 & 1 & 0 & 0 & 0 \\ 0 & 0 & 1 & 0 & 0 \\ 0 & 0 & 0 & 1 & 0 \\ 0 & 0 & 0 & 0 & 1 \\ 0 & 0 & 0 & 0 & 1 \\ 0 & 0 & 0 & 0 & 1 \\ 0 & 0 & 1 & 0 & 0 \\ \cdots & \cdots & \cdots & \cdots & \cdots \end{bmatrix} \tag{2.23}$$

Then it is obvious that we relate V_{xy} and $\boldsymbol{y}$ to $\hat{V}_{xy}$ and $\hat{\boldsymbol{y}}$ by

$$\hat{\boldsymbol{y}} = Q\boldsymbol{y}, \quad \hat{V}_{xy}Q = QV_{xy}. \tag{2.24}$$

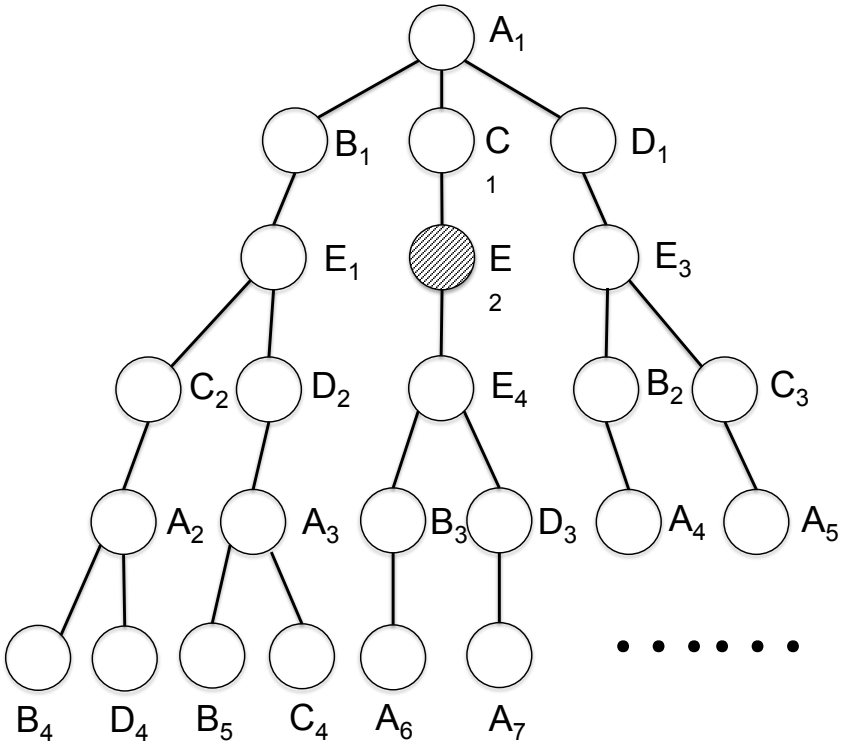

Figure 2.4: Modified unwrapped tree $\hat{G}'$ from node A. Nodes with shade are buffered node added to emulate when error occurs, which have the same statistics as the one it is derived from.

It can be seen that $\hat{\boldsymbol{y}}$ and $\hat{V}_{xy}$ are copies of rows in $\boldsymbol{y}$ and V_{xy}. However, $\hat{V}_{xx}Q \neq QV_{xx}$, because for leaf node $\hat{x}_j$, $\hat{V}_{xx}(i,j)$ is not simply copied from $V_{xx}(I,J)$. This is because that, a $k-degree$ node in G has k neighbors, while the corresponding nodes located in the leaves of the unwrapped tree do not have children. This leads to the difference between $\hat{V}_{xx}(i,j)$ and $V_{xx}(I,J)$.

Thus we need to consider this error when relating both quantities:

$$\hat{V}_{xx}Q + \Delta = QV_{xx} \tag{2.25}$$

where Δ is an error matrix whose first $m-l$ rows are zero, referring to $m-l$ non-leaf nodes where l is the number of leaf nodes in the unwrapped graph.

Now we have known some basic relations between the original cyclic graph and the unwrapped tree. We thereby give two lemmas, which show how G and $\hat{G}$ are related with

proof provided in the appendix. Without the loss of generality, we set the root of unwrapped tree to be x_1 and its connected observed version y_1.

Lemma 2.1. *Let $\mu(1)$ be the correct mean of node 1, and $\hat{\mu}(1)$ be the conditional mean of root node 1 after T iterations, where T is the depth of the unwrapped tree, then*

$$\hat{\mu}(1) = \mu(1) + \hat{C}_{x_1|y}\Delta\mu \tag{2.26}$$

where $\hat{C}_{x_1|y}$ is the first row of $\hat{C}_{x|y}$ or $\hat{V}_{xx}^{-1}$, and Δ is an error matrix whose first $M-l$ rows are all zero. None zero part of Δ corresponds to the leaf nodes in $\hat{G}$.

Proof. See Appendix A □

Lemma 2.1 gives the difference between $\mu(1)$ and $\hat{\mu}(1)$.

Lemma 2.2. *Let $\sigma^2(1)$ be the correct variance of node 1 and $\hat{\sigma}^2(1)$ be the conditional variance of node 1 after T iterations, where T is the depth of the unwrapped tree, then*

$$\hat{\sigma}^2(1) = \sigma^2(1) + \hat{C}_{x_1|y}\Delta C_{x_1|y}^T - \hat{C}_{x_1|y}r \tag{2.27}$$

where Δ is the error matrix as described in Lemma 2.1 and the vector r has value 1 for element that corresponds to node 1 in the original cyclic graph G and value 0 elsewhere.

Proof. See Appendix B □

Lemma 2.2 provides the difference between $\sigma^2(1)$ and $\hat{\sigma}^2(1)$.

To prove that BP converges to the correct fixed point, we must show that the residue term and the error term in Lemmas 2.1 and 2.2 are bounded and vanish with the iteration. From Lemmas 2.1 and 2.2, we can easily see that both $\Delta\mu$ and $\Delta C_{x_1|y}^T$ are bounded, since only the last l rows in E are non-zero while μ and $C_{x_1|y}^T$ have fixed values independent of the iterations. Therefore we can give the following theorem with easy proof described as above:

Theorem 2.3. *Assume that the conditional correlation between the root node and leaf nodes in the unwrapped tree decreases sufficiently fast, i.e. $\forall\ \epsilon > 0$, $\exists\ T_\epsilon = f(\epsilon)$ such that $\forall t > T_\epsilon$ $|\hat{C}_{x_1|y}\Delta\mu| < \epsilon \max_{i\in[1,m]} |\Delta\mu|$. Then we have (1) BP converges (2) the expectation μ is*

exact while the variances are equal to the true variances minus the summation of conditional correlations between root node $\hat{x}_1$ and all other nodes $\hat{x}_j$ that are copies of x_1.

However, in reality it is difficult to tell whether the conditional correlation between the root node and leaf nodes decrease sufficiently fast. We can only tell whether BP converges to a fixed point of BP assignment. In the GMRF case, due to the special property of exponential functions, we can get better results. We first propose Lemma 2.4, from which we will reach the final conclusion in Theorem 2.5

Lemma 2.4. *If ϕ is a fixed point of the BP in G, then we can expand G to construct an unwrapped tree $\hat{G}$ such that (a) all non-leaf nodes in $\hat{G}$ have the same statistical relationship with neighbors as the corresponding nodes in G, with the exception of the virtual buffer nodes; (b) all nodes in $\hat{G}$ have the same beliefs as the those obtained at the fixed point ϕ in G.*

Proof. See Appendix C. □

With Lemma 2.4, we can prove Theorem 2.5:

Theorem 2.5. *For an arbitrary Gaussian graphic model, if ϕ is a fixed point resulted by BP subjected to possible message passing failure, the resulted expectations from this fixed point are exact.*

Proof. See Appendix D. □

So far, we have shown that, given sufficient iterations, if BP converges to some fixed point, then the loopy expectations based on this point are correct. In fact, there are cases [25] where some fixed points exist but the expectation does not converge to the exact value.

Therefore in our cooperative spectrum sensing scenario with static primary user, if BP converges to a fixed point, then this point will yield correct expectations and the same decisions as those without communication errors. In the scenario where PU is dynamic, due to the limited number of iterations and up-to-date local observations, we cannot guarantee the convergence; however, the numerical results show that the proposed algorithm does work in practice, which can be justified by our theoretical analysis to some extent.

2.5.2 Performance Analysis of Cooperative Quickest Detection

Quickest detection, as an efficient technique to detect the change in sample distribution, has been widely used in many fields such as process control, financial decision and statistical signal processing, especially CUSUM test, one of the most widely used algorithms for quickest change detection. For centralized detection, the central node which is the only decision maker, claims a change by giving the stopping time T^*, as defined in equation (2.14) and (2.15),

$$T^* = \inf\{t \geq 0 | s^k(t) \geq \gamma\}, \gamma \geq 0$$

$$s^k(t) = \max_{k \leq j \leq t} \left\{ \sum_{r=j}^{t} l(r) \right\}$$

by Page's Procedure [28], the above equations are equivalent to equation (2.28) and (2.29)

$$T^* = \inf\{T(k), k = 0, 1, 2, \cdots\} \tag{2.28}$$

$$T(k) = \inf \left\{ t | \sum_{r=k}^{t} l(r) \geq \gamma \right\}, \ \gamma \geq 0 \tag{2.29}$$

Here, we assume the pre-change and post-change distributions f_0 and f_1 are known. The CUSUM stopping time T^* has been proved to achieve the optimal solution in terms of minimum delay [24][32]. However, in the case of bounded threshold, it is difficult to give explicit performance measures and analysis. But we can analyze the case of sufficiently large threshold or equivalently with sufficiently large samples with Brownian motion approximation, which is commonly used to help analyze continous system [34][37], since

$$\hat{b(t)} \triangleq \frac{\sum_{r=0}^{Nt}(l(r) - E[l(r)])}{\sqrt{N}} \tag{2.30}$$

converges to a Brownian motion with drifting rate $\hat{\mu} = 0$, and variance $\hat{\sigma}^2 = V[l(r)]$, when $N \to \infty$. And the threshold will accordingly be $\hat{\gamma} = \gamma/\sqrt{N}$. Then $\sum_{r=0}^{Nt} l(r)/\sqrt{N}$ can be approximated by $b(t)$ with $\mu = \sqrt{N}E[l(r)]$ and $\sigma^2 = \hat{\sigma}^2 = V[l(r)]$, $\hat{\gamma} = \gamma/\sqrt{N}$.

Then, t^* that corresponds to T^* defined in equation (2.14) can be expressed as below:

$$t^* = \inf\{t | b(t) - \min_{0 \le k \le t} b(k) \ge \hat{\gamma}\} \tag{2.31}$$

In this chapter we look into two average run lengths (ARLs) as the performance criteria for quickest detection, as used in many other theoretical materials [24][10]. These two ARLs are given by

$$\mathcal{D}_i = esssup(E_t | T_i^* - t | \mathscr{F}_{t-1}), \quad \mathcal{F}_i = E_\infty[T_i^*] \tag{2.32}$$

where E_t means the expectation under the condition that the change occurs at time t, while E_∞ gives the expectation under the assumption that the change never happens. T_i^* is the stopping time of node i and $\mathscr{F}_{t-1}$ is the filtration or history before $t-1$ (including $t-1$). Thus we define $\mathcal{D}_i$ as the indicator of detection delay on node i and $\mathcal{F}_i$ the means average time elapsed between two false alarms. Since small detection delay and small false alarm rate mean a good performance, small $\mathcal{D}$ and large $\mathcal{F}$ are expected for a good detection algorithm.

It is shown by Brownian motion approximation based asymptotic analysis [15] that in CUSUM test, with sufficiently large threshold $\hat{\gamma}$, $\mathcal{D}$ and $\mathcal{F}$ can be approximated by

$$E[t^*] \approx \begin{cases} \dfrac{\hat{\gamma}}{\mu} & \mu > 0 \\ \dfrac{\sigma^2}{2\mu^2} \exp\left(-\dfrac{2\mu\hat{\gamma}}{\sigma^2}\right) & \mu < 0 \end{cases} \tag{2.33}$$

$$\begin{cases} \mathcal{D} \approx N \cdot E[t^*] & \mu > 0 \\ \mathcal{F} \approx N \cdot E[t^*] & \mu < 0 \end{cases} \tag{2.34}$$

which agrees with the intuition that a larger threshold results in larger delay but smaller false alarm rate.

In our cooperative spectrum sensing scenario, however, there is no central node. Therefore we need to see how each node conducts the CUSUM test with likelihood ratios passed from its neighbors. First let us consider a two-node (denoted by A and B) scenario where each node make decision based on ifself and the other one, and assume nonzero communication

delay but no communication errors, and both nodes are perfect synchronized. By adopting the Page's procedure in equations (2.28) and (2.29) , we modify the sum $\sum_{r=k}^{t} l(r)$ at node A as below in equation (2.36) as well as the stopping time at node A:

$$T_A^* = inf\{T_A(k), k = 0, 1, 2, \cdots\}, \tag{2.35}$$

$$\begin{aligned} T_A(k) =& inf\{t | s_A^k(t) \geq \gamma_A\}, \\ s_A^k(t) =& \sum_{r=k}^{t} l_A(r) + \sum_{r=k}^{t-D} l_B(r) \end{aligned} \tag{2.36}$$

where D is communication delay between the two nodes, while l_A and l_B are the log-likelihood ratios of H_1 versus H_0 at node A and B, respectively. Intuitively, the second summation does not include summation from $l_B(t - D + 1)$ to $l_B(t)$ because at time t node A can only receive some past information that node B had, due to the communication delay D. If we consider the LLR as two parts, the first part α consists of those obtained before time slot $t - D$, the other part β consists of those from time slot $t - D + 1$ to t, where

$$\alpha = \sum_{r=k}^{t-D} l_A(r) + l_B(r) \qquad \beta = \sum_{r=t-D+1}^{t} l_A(r) \tag{2.37}$$

Then we have stopping times for two stages given by

$$\begin{aligned} T_A^{\alpha} =& inf\{T_A(k), k = 0, 1, 2, \cdots, t - D\}, \\ T_A^{\beta} =& inf\{T_A(k), k = t - D + 1, \cdots, t\} \end{aligned} \tag{2.38}$$

It is obvious that the stopping time T_A^* can be represented by T_A^{α} and T_A^{β}:

$$T_A^* = \min(T_A^{\alpha}, T_A^{\beta}) \tag{2.39}$$

Then we define the following terms to facilitate the performance analysis:

$$\begin{aligned} I_i \triangleq E_r[l_i(r)], \quad J_i \triangleq E_{\infty}[l_i(r)], \quad i = A, B \\ U_i \triangleq V_r[l_i(r)], \quad W_i \triangleq V_{\infty}[l_i(r)], \quad i = A, B \end{aligned} \tag{2.40}$$

$$R_A(t) = \sum_{k=1}^{t} l_A(k) + \sum_{k=1}^{t-D} l_B(k), \tag{2.41}$$

where I_i is the K-L divergence $D(f_i^{(1)}||f_i^{(0)})$, and $J_i = -D(f_i^{(0)}||f_i^{(1)})$. Then by Wald's Identity [41], we have

$$\begin{aligned} E[R_A(T)] &= E\left[\sum_{k=1}^{T} l_A(k)\right] + E\left[\sum_{k=1}^{T-D} l_B(k)\right] \\ &= E[T]E[l_A(k)] + E[\max(T-D,0)]E[I_B(k)] \\ &= I_A E([T] + I_B[E[\max(T-D,0)] \end{aligned} \tag{2.42}$$

We assume that time slot D in the discrete system is equivalent to time $t = 1$ in the Brownian motion and thus t_A^* satisfies

$$T_A^* \approx D \cdot t_A^* \tag{2.43}$$

Applying equation (2.42) at stopping time T_A^* and ignoring the overshoot, we have $R_A(T_A^*) \approx \gamma_A$ thus we can obtain an extended Wald's approximation of γ

$$\gamma_A \approx I_A E[T_A^*] + I_B E[\max(T_A^* - D, 0)] \tag{2.44}$$

It can be difficult to decouple T_A^* from the expectation $E[\max(T_A^* - D, 0)]$ in Eq. (2.44). However, using Brownian motion approximation, it can be proved [15] that for sufficiently large D, it is highly possible that, if $I_A D > \gamma_A$, γ_A can be hit between time slot 0 to time slot D, or time interval $t = [0, 1]$ in terms of the Brownian motion approximation; and with a high probability, if $I_A D < \gamma_A$, the threshold cannot be reached. From this result we have

$$P(T_A^* < D) \xrightarrow{\gamma_A \to \infty} \begin{cases} 1, & \text{if } I_A D > \gamma_A \\ 0, & \text{if } I_A D < \gamma_A \end{cases} \tag{2.45}$$

$$\frac{\max(T_A^* - D, 0)}{D} \xrightarrow{\mathcal{P}} \begin{cases} 0, & \text{if } I_A D > \gamma_A \\ \dfrac{T_A^* - D}{D}, & \text{if } I_A D < \gamma_A \end{cases} \tag{2.46}$$

Therefore, for sufficiently large D, we have the following estimation of ARL $\mathcal{D}$ at node A by combining equation (2.34) (2.43) (2.44) (2.46) :

$$\mathcal{D}_A = \begin{cases} \dfrac{\gamma_A}{I_A}, & \text{if } I_A D > \gamma_A \\ \dfrac{\gamma_A + I_B D}{I_A + I_B}, & \text{if } I_A D < \gamma_A \end{cases} \tag{2.47}$$

from which we could see when the threshold at a node is not large enough, information passed from its neighbor node does not contribute much to the quickest detection performance $\mathcal{D}$. However, we can adjust the threshold such that the trade-off between $\mathcal{D}$ and $\mathcal{F}$ can be achieved.

For $\mathcal{F}$, again due to the difficulty in the analysis of finite systems, using the same Brownian motion approximation as used for the analysis of $\mathcal{D}$, we have the following asymptotic approximation for $\mathcal{F}$ when γ is large, as $\gamma \to \infty$,

$$\log \mathcal{F}_A \geq \tfrac{2|J_A+J_B|\gamma_A}{W_A+W_B} - \tfrac{2|J_A+J_B|J_A}{W_A+W_B} - \tfrac{2(J_A+J_B)^2 W_A}{(W_A+W_B)^2} \tag{2.48}$$

where J_A, J_B, W_A, W_B are defined in Eq. (2.40). Due to the page limit, we do not provide the proof of (2.48) here. In the case of Gaussian distribution, for example, for node i, $H_0 \sim N(\mu_0^i, 1)$ and $H_1 \sim N(\mu_1^i, 1)$, it is straightforward to examine [32]

$$\begin{gathered} I_A = -J_A = (\mu_1^A - \mu_0^A)^2,\ I_B = -J_B = (\mu_1^B - \mu_0^B)^2, \\ U_A = 2I_A,\ U_B = 2I_B. \end{gathered} \tag{2.49}$$

Substituting (2.49) into (2.48), we have

$$As\ \gamma_A \to \infty,\ log(\mathcal{F}_A) \geq \gamma_A \tag{2.50}$$

Furthermore we can show that the equality holds asymptotically in Eq. (2.50).

Theorem 2.6. *If the distributions are Gaussian and Brownian motion approximation holds, we have*

$$log(\mathcal{F}_A) = \gamma_A = I_A \mathcal{D}_A + I_B \max(\mathcal{D}_A - D, 0) \quad as\ \gamma_A \to \infty, \tag{2.51}$$

Proof. See Appendix E. □

Theorem 2.6 shows the relationship between $\mathcal{F}_A$ and $\mathcal{D}_A$, which also characterizes the tradeoff between them.

After the analysis of the two-node network, we can now move to the more general case where multiple nodes exist. For a network topology of N nodes, denote by $\phi_A^{(n)}$ the set of nodes that are n hops away from node A, and $N(A)$ the neighbor nodes of A, which is equivalent to $\phi_A^{(1)}$.

Similar to the two-thread CUSUM test and the stopping times as in (2.35) to (2.39), we have

$$T_A^* = \min(T_A^0, \cdots, T_A^{n-1}) \tag{2.52}$$

where $n = W/D$, and W is the window size out of which observations received from other nodes will not be used. $\forall i = 1, \cdots, n-1$,

$$T_A^i = \min\left(t \left| s_A^i(t - iD) + \sum_{j=0}^{i-1} \sum_{\theta \in \phi_A^{(j)}} \sum_{r=t-iD+1}^{t-jD} l_\theta(r) \geq \gamma_A \right. \right) \tag{2.53}$$

where

$$s_A^i(t) = \max\left(s_A^i(t-1) + \sum_{j=0}^{n} \sum_{\theta \in \phi_A^{(j)}} l_\theta(t), 0 \right) \tag{2.54}$$

For $i = 0$,

$$T_A^0 = \min\left(t \left| \max_{t-D+1 \leq k \leq t} \sum_{r=k}^{t} l_\theta(r) \geq \gamma_A \right. \right) \tag{2.55}$$

We could easily check that the two node system is a special case of the multiple nodes. Similarly to (2.51) we can obtain the asymptotic equation for node A in multi-node network as (2.56) in the following theorem:

Theorem 2.7. *For the generic case of multiple-node networks, we have*

$$I_A \mathcal{D}_A + \sum_{i=1}^{n} \left(\sum_{\theta \in \phi_A^{(i)}} I_\theta \right) \max(\mathcal{D}_A - iD, 0) = \log \mathcal{F}_A \tag{2.56}$$

as $\gamma_A \to \infty$, where I_θ is the K-L divergence of node θ as defined in (2.40).

2.6 Numerical Results

In this section, we use numerical simulation results to demonstrate the performance of the proposed BP based quickest cooperative spectrum sensing and compare it with that of traditional detection with BP. We set the total SU number $N = 400$. The SUs are randomly distributed in a $4000m \times 4000m$ square area. A PU follows a sine curve path starting from $(-2000, 0)$, with the constant horizontal velocity $V_x = 36km/h$. Assume that each iteration in the BP procedure takes $100ms$, which we define as one time slot. The primary user impact range R is set to 1000m, and the maximum communication distance between SUs is set to $D = 200m$. The power of PU is $P = 20W$, which is 43.01 dBm. The received power observation Y_i, affected by path loss and shadow fading, is calculated by the following model with path loss exponent $\gamma = 3.5$:

$$Y_i = P - 28.6 - 35log_{10}d_i + P_n \ , \tag{2.57}$$

where d_i is the distance between the i^{th} SU and the PU, P_n is Gaussian random noise (caused by log normal shadow fading) with variance σ_n^2, and X_{edge} is computed by having $d_i = R$; i.e.,

$$X_{edge} = P - 28.6 - 35log_{10}R \tag{2.58}$$

And all the simulation results are based on 100 realizations of the configurations mentioned above, and during each realization, the PU moves through the above-mentioned square area at the designated speed. We tested over various message transmission error rate e, window length L (which is defined in the last part of Section 2.4) and noise variance σ_n^2. For clarity we define a false alarm as claiming a change either from H_0 to H_1 or H_1 to H_0 while actually the change has not happened. Then we can use the receiver operating characteristic (ROC) curve in terms of false alarm rate[2] and average detection delay to measure the performance,

[2]The false alarm rate in the simulation result is defined as (Number of false alarm among all SUs during the simulation)/(Length of simulation $\times$ number of SUs)

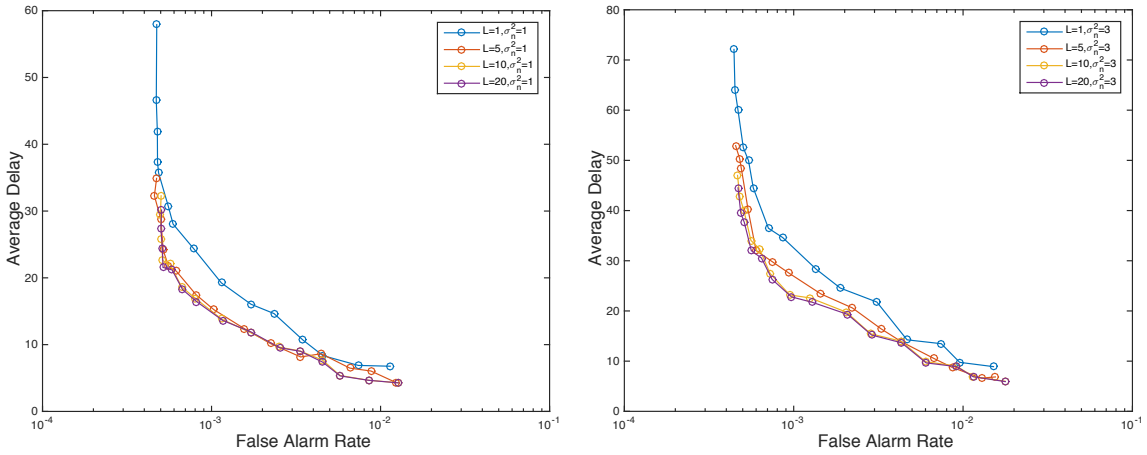

Figure 2.5: ROC curves at different window sizes L

which corresponds to the two ARLs mentioned in (2.32). Here we use false alarm rate instead of ARL because H_0 can mean many different scenarios depending how far the SU is from the PU, so statistically the simulated false alarm rate is inversely proportional to the ARL $\mathcal{F}_i$. Besides the assumptions made in Section 2.2, we also make the following reasonable assumptions:

- We only consider packet losses incurred by communication failure and do not consider quantization error in communications.
- We ignore the missed detection, where a change occurs without being detected. This is because for quickest detection, ideally a change can always be detected given sufficient long time. It is very unlikely that the PU enters a SU's alert range and leaves immediately, in which case the SU cannot detect the presence of PU for the lack of observations.
- All SUs receive incoming messages and update the belief messages simultaneously, such that we do not specify sensing and processing intervals.

To determine the window length L, we tested different Ls under various noise levels, as shown in Fig. 2.5. Here $L = 1$ means the traditional detection method. It can be seen that the performance gap becomes unnoticeable when $L \geq 10$. Considering the computation and communication cost of maintaining the size L window, we choose $L = 10$ in our algorithm.

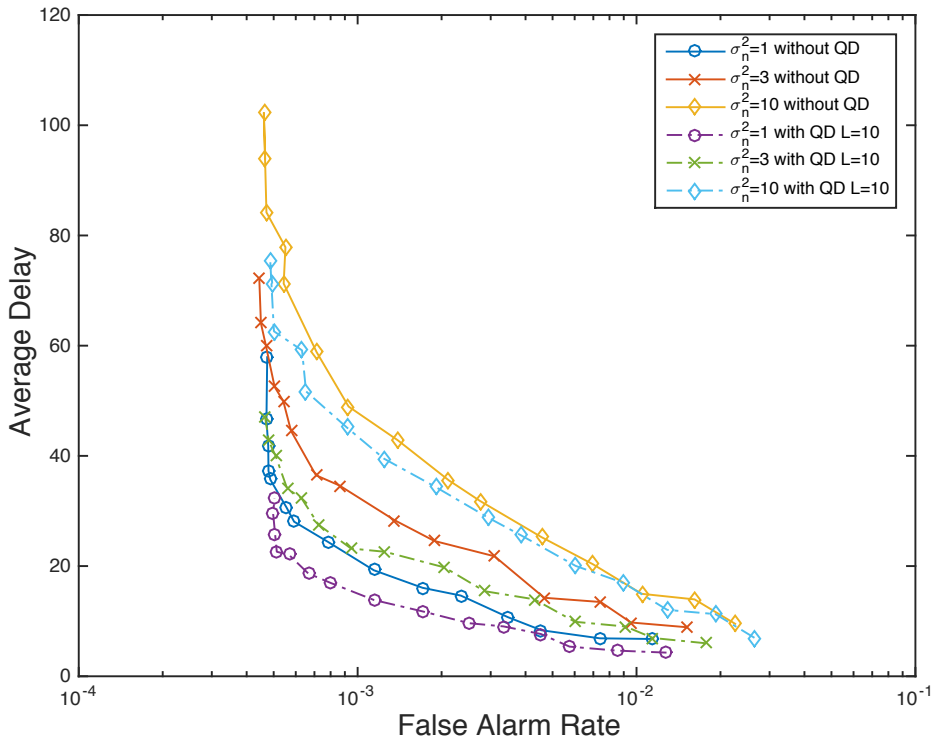

Figure 2.6: ROC curves at different noise levels with window length $L = 10$

Fig. 2.6 shows a comparison between BP based traditional detection which is equivalent to quickest detection with window length $L = 1$, and the BP based quickest detection of window length $L = 10$ in terms of the ROC curves under different noise levels. The dash lines represent the ROCs with quickest detection, and solid lines represent the traditional method. It can be seen that the proposed quickest detection outperforms the traditional BP based detection without the quickest detection.

We also test our proposed spectrum sensing algorithm with setups of different message passing error rates. Fig. 2.7 gives performance under error rate 100%, 20% and 0% for two different fading levels. In our simulation, since the PU is moving, when an error occurs, the same belief message will not be sent again. Therefore the SU will approximately replace the otherwise received correct message with its own priors when computing the next belief messages and updating its own belief.

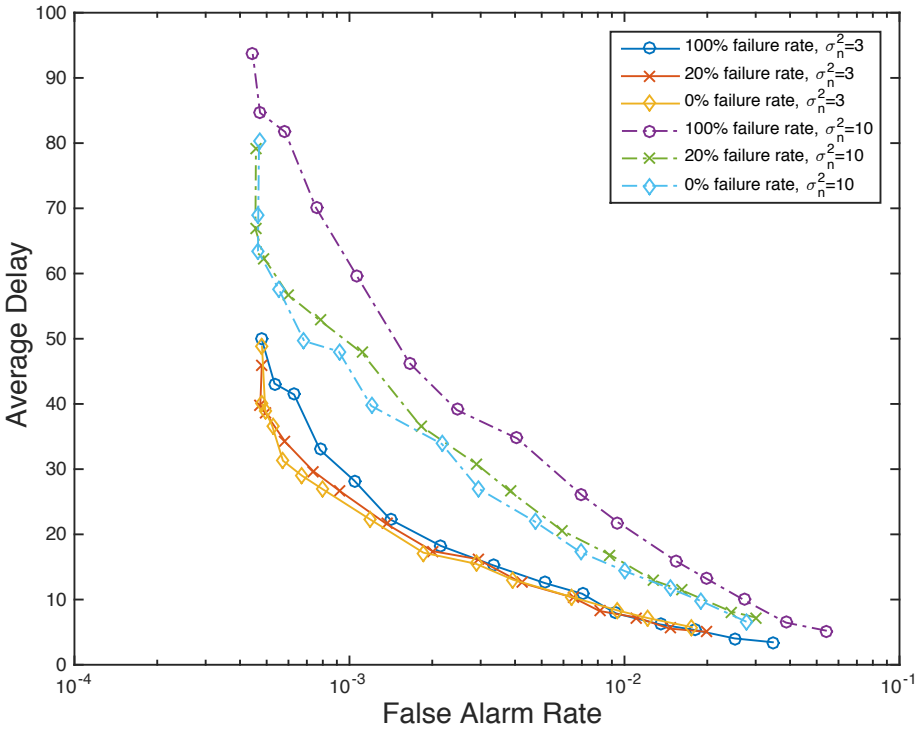

Figure 2.7: ROC curves with different communication error rates

We can also see from Fig. 2.7 that, when the communication failure rate is low, the ROC can be very close to that of no error case. This agrees with the conclusion in Section 2.5, which states that BP can empirically "converge" even when message loss happens. We say the convergence is empirical because with finite iterations, the loopy BP in the GMRF cannot converge and to the correct expectation. However, under our assumption that "if the conditional correlation between the root node and leaf nodes in the unwrapped tree decreases sufficiently fast", we claim that it "converges" empirically. Fig. 2.8 illustrates the convergence process on an SU when PU is static.

2.7 Conclusion

In this chapter, we have discussed the BP framework used for cooperative spectrum sensing, into which the CUSUM quickest detection is integrated. The impact of possible message passing failure on BP convergence has been analyzed. The finite length approximations of CUSUM quickest detection and distributed quickest detection have been theoretically

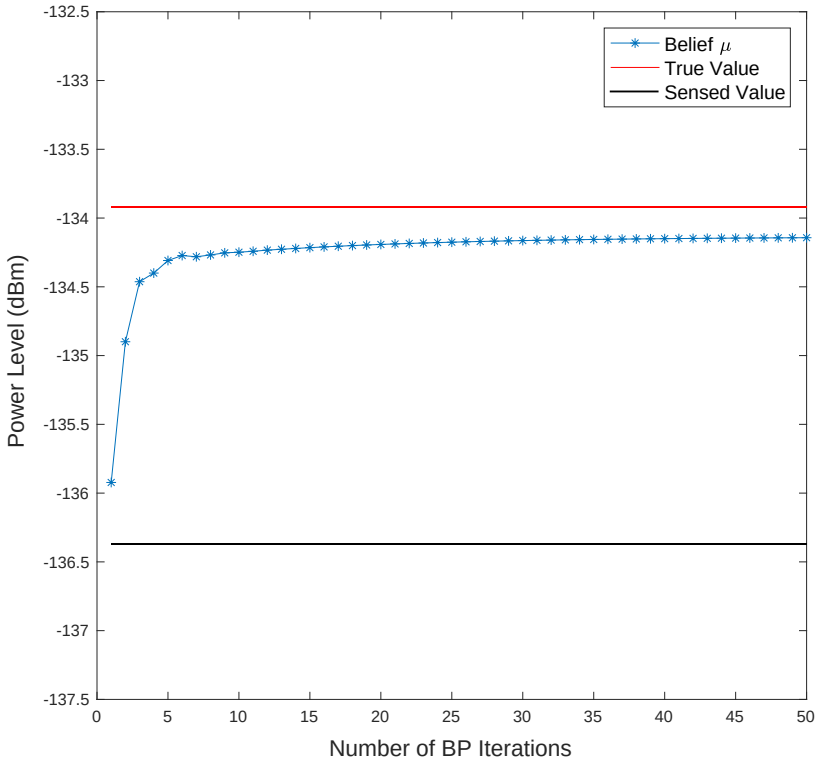

Figure 2.8: BP convergence illustration

analyzed. Numerical results have shown that our proposed BP based quickest detection algorithm can achieve a better detection performance in terms of delay and false alarm rate when compared with traditional spectrum sensing approach.

Part II

Universal Quickest Detection

Chapter 3

Universal Quickest Spectrum Sensing

This chapter is revised based on a conference paper by Yifan Wang and Dr. Husheng Li:

Wang, Y., & Li, H. (2016). Universal Quickest Spectrum Sensing. In *2016 IEEE Global Communications Conference (GLOBECOM)* (pp. 1-6). IEEE.

Abstract

In modern cognitive ratio systems, the spectrum is becoming increasingly crowded and expensive; thus spectrum sensing becomes more important than ever before. Traditional spectrum sensing assumes Gaussian noise (or of other given distributions) in general. However, when secondary users (SUs) have no prior information about the measurement distributions, the spectrum sensing schemes assuming given distribution forms (even if the parameters are assumed to be unknown) no longer apply. In this chapter we propose a universal quickest change detection scheme based on density ratio estimation for spectrum sensing by detecting the sudden change of spectrum (e.g., the emergence of primary user), where neither the pre- change nor post-change distribution (even the distribution forms) is known to SUs, thus achieving robustness to complex spectrum environment.

3.1 Introduction

In cognitive radio systems, one of the key techniques, as well as design goals, is the spectrum sensing, which has substantial impact on the applicability of cognitive radio in the future. As wireless communication technology advances, the spectrum is becoming increasingly crowded and expensive. By spectrum sensing this valuable resource can be more efficiently utilized. Generally speaking, spectrum sensing is to detect spectrum activities, such that secondary users (SUs) without license to the frequency band (which is licensed to primary users (PUs)) can then be able to use this band to communicate with each other, when PUs are not present. In other words, SUs should be agile and have robust awareness of the presenfce or absence of PUs with acceptable detection delay and false alarm rate.

One efficient approach for the spectrum sensing is to apply the abrupt change point detection [32, 20], which is coined quickest spectrum sensing [18, 13]. Such an approach

considers the sensed signal at SU as a random process and tries to detect the time when the PU's status is changed, either from absence to presence or vice versa. The abrupt change detection problem has been substantially studied for many years, among which the likelihood ratio (LR) based Cumulative Sum (CUSUM) test or the Page's procedure [28] is shown to be optimal (in terms of detection delay and false alarm rate) under Lorden's criterion. Most of the related studies in the area of change detection fall into the settings where the distributions before and after the change are known or partially known [8, 18, 13]. When the distributions are unknown, [13, 40] provide guidance for non-parametric robust quickest detection, where neither the pre-change nor post-change distribution is exactly known, while both are assumed to be of some known family of distributions, i.e. with known form but unknown parameters (e.g., Gaussian distributions with unknown expectations). However, to the authors' best knowledge, there is no existing research on the quickest detection in the context where both the pre-change and post-change distributions are completely unknown (including both distribution families and parameters). In the circumstance where we only have data samples (the sensing observations in spectrum sensing), we need to fully exploit the data for detecting the change.

In this chapter, we'll first compare two non-parametric approaches, the nearest neighbor divergence estimation [42] and Kullback-Leibler Importance Estimation Procedure (KLIEP) [36] for change detection with no prior information of the post-change and pre-change distributions. Since they don't rely on any prior information of the distribution, we call them universal spectrum sensing. Then we will combine the importance estimation with the CUSUM quickest detection. Both approaches are essentially observations driven density ratio estimation. This is to avoid non-parametric density estimation that is notoriously difficult for its heavy computational complexity [9]. With the estimated density ratio, we can then compare the incoming observations with existing ones serving as reference or training data, such that a SU can detect the change of the PU status.

The remainder of this chapter is organized as follows. In Section 3.2, the detection problem is formulated and modeled. In Section 3.3 the two density ratio estimation schemes are introduced followed by our proposed detection procedure. Section 3.4 provides an

asymptotic performance analysis. Numerical results are provided in Section 3.5, and the conclusion is given in Section 3.6

3.2 Problem Statement and Modeling

For analysis simplicity, we assume energy detection for spectrum sensing. However, the principle can be extended to other statistical detection schemes for spectrum sensing. In the model of this chapter, a SU detects the existence of active PU only when the power level of sensed signal is larger than some threshold. Hence, we can model this problem as a change point detection problem. We assume that the sensed signal power at SU is a sequence of independent and identically distributed (i.i.d.) random variables $\{X_i, i = 1, 2, 3, \dots\}$, and that there are two possible distributions F_0 and F_1 for X_i. This is formulated in (3.1), where T_C is the change point such that $\{X_i, i < T_C\} \sim F_0$, and $\{X_i, i \geq T_C\} \sim F_1$.

$$\begin{cases} X_i \sim F_0 & \text{for} \quad i < T_C \\ X_i \sim F_1 & \text{for} \quad i \geq T_C \end{cases}. \tag{3.1}$$

Note that we don't specify the detailed expression of F_0 and F_1, since we assume that we don't have the prior information except for $F_0 \neq F_1$. In practice, F_0 is the distribution of noise while F_1 is that of signal plus noise.

We denote by τ the time that a change is detected (which could turn out to be a false alarm). Our goal is to detect T_C with the minimum worst-case detection delay D_W given a constraint on the false alarm probability P_{FA}:

$$\begin{aligned} &\min D_W(\tau) \\ \text{subject to} \quad &P_{FA} \leq \alpha, \end{aligned} \tag{3.2}$$

where α is the constraint on the false alarm rate and

$$D_W(\tau) = \sup_{T_C \geq 1} ess\sup E^{T_C}[(\tau - T_C + 1^+)|\mathcal{F}_{T_C - 1}], \tag{3.3}$$

where $\mathcal{F}_t$ is the σ-field generated by $X_1, X_2, \cdots, X_t$.

If both F_0 and F_1 are known distributions with known parameters, it is easy to detect the change point with the LR approach. Under the Lorden criterion [20], the CUSUM test is proved to be the optimal solution (even for nonasymptotic case!) to the minimax detection problem (3.3), the stopping time of which minimizes the D_W given an upper bound of P_{FA}. The time to claim the change in the CUSUM test is given by

$$\tau^* = \inf \left\{ t \geq 1 : \max_{1 \leq k \leq t} \sum_{i=k}^{t} l(X_i) \geq \gamma \right\} \tag{3.4}$$

where γ is selectet such that $E_0(\tau^*) = 1/\alpha$.

However, in our setup both F_1 and F_0 are unknown due to lack of knowledge about noise type, wireless channels and PU signal. We can't calculate the log-LR $l(X_i)$ thus have to seek other methods that don't require direct calculation of LR.

We assume that the first M observations in the sequence $\{X_i\}_i$ are known to be subject to F_0. Then, we can use them as the training data, denoted by $\boldsymbol{X}_{tr}$. This assumption is reasonable; otherwise, it is possible that there is no (or very little) data generated from F_0, which makes the change detection impossible. We denote by $\boldsymbol{X}_{te}$ the testing data, which is a subsequence in X_i from $i = t_{te}$ to $i = t$. Our hypotheses are as follows:

$$\begin{cases} H_0 : P(\boldsymbol{X}_{te}) = P_0(\boldsymbol{X}_{te}) \\ H_1 : P(\boldsymbol{X}_{te}) = P_1(\boldsymbol{X}_{te}) \end{cases} \tag{3.5}$$

The LR of H_1 over H_0 can be written as

$$\boldsymbol{\Lambda}(t) = \frac{P_1(\boldsymbol{X}_{te})}{P_0(\boldsymbol{X}_{te})} = \prod_{i=t_{te}}^{t} \frac{P_1(X_i)}{P_0(X_i)}, \tag{3.6}$$

or in terms of logarithm LR,

$$\boldsymbol{\lambda}(t) = \log \frac{P_1(\boldsymbol{X}_{te})}{P_0(\boldsymbol{X}_{te})} = \sum_{i=t_{te}}^{t} \log \frac{P_1(X_i)}{P_0(X_i)} = \sum_{i=t_{te}}^{t} l(X_i). \tag{3.7}$$

Our problem is to estimate $\boldsymbol{\lambda}(t)$ without knowing P_1 and P_0. In the next section, we will compare two non-parametric approaches to estimate the LR that are mentioned above.

3.3 Non-parametric Quickest Detection

In this section, two non-parametric approaches will be discussed when they are used for the estimation of the log-LR between two sets of data, as $\boldsymbol{\lambda}(t)$. This log-LR between testing data and training data is essentially related to the Kullback-Leibler (K-L) divergence, which can be defined as in (3.8). If we assume that the testing data $\boldsymbol{X}_{te}$ is subject to F_1, and the training data is of F_0, then the K-L divergence from F_1 to F_0 is given by

$$D(F_1\|F_0) = \int_{\mathbb{R}} \mathrm{d}F_1 \log \frac{\mathrm{d}F_1}{\mathrm{d}F_0}. \tag{3.8}$$

We denote by f_1 the density of F_1 and f_0 the density of F_0, based on which the divergence from F_1 to F_0 can be written as

$$D(f_1\|f_0) = \int_{\mathbb{R}} f_1(x) \log \frac{f_1(x)}{f_0(x)} \mathrm{d}x. \tag{3.9}$$

In the discrete value case, Eq. (3.9) can be rewritten as

$$D(P_1\|P_0) = \sum_{x\in\boldsymbol{X}_{te}} P_1(x) \log \frac{P_1(x)}{P_0(x)}. \tag{3.10}$$

By the law of large numbers, it can be further simplified to

$$D(P_1\|P_0) = \frac{1}{N} \sum_{x\in\boldsymbol{X}_{te}} \log \frac{P_1(x)}{P_0(x)} = \frac{\boldsymbol{\lambda}}{N}, \tag{3.11}$$

as $N \to \infty$, where N is the number of samples in $\boldsymbol{X}_{te}$. Hence we can see the relationship between $\boldsymbol{\lambda}$ and the K-L divergence.

3.3.1 Nearest Neighbor Approach

Since we need to compute the metric $\boldsymbol{\lambda}$ for the hypothesis test in (3.5), we can either estimate $P_0(\boldsymbol{X}_{te})$ and $P_1(\boldsymbol{X}_{te})$ separately and compute the density ratio Λ and λ, or directly estimate the ratio itself. There are many ways to estimate probability density from data, such as the k-NN approach; however, it is well known that the computational complexity is very high. Therefore, we have to explore the latter option, namely directly estimating the density ratio.

In [42], a nearest-neighbor based estimator is given to estimate the K-L divergence between two random vectors. The idea behind this is based on k-NN density estimate, given by

$$\hat{P}_k(x) = \frac{k}{(N-1) \cdot V_{x,k}}, \tag{3.12}$$

where N is the number of samples used to estimate the density $P(x)$, and $V_{x,k}$ is the volume of the ball with radius equal to the distance between its center x and its k-nearest neighbor. Then from (3.11) we define $\hat{P}_{1_k}(x)$ and $\hat{P}_{0_k}(x)$ as follows:

$$\hat{P}_{1_k}(X_i) = \frac{k}{(N-1) \cdot V_{X_i,k}}, \quad \hat{P}_{0_k}(X_i) = \frac{k}{M \cdot V'_{X_i,k}} \tag{3.13}$$

where $V_{X_i,k}$ is the volume of the ball $B(X_i, \rho_N(i))$, $V'_{X_i,k}$ is the volume of the ball $B(X_i, v_M(i))$, and when $k = 1$, ρ_N and v_M are defined as

$$\begin{aligned} \rho_N(i) &= \min_{j=t_{te},\ldots,t, j\neq i} \|X_i - X_j\|, \ for\ i = t_{te}, \ldots, t \\ v_M(i) &= \min_{j=1,\ldots,t_{tr}} \|X_i - X_j\|, \ for\ i = t_{te}, \ldots, t \end{aligned} \tag{3.14}$$

$$\hat{P}_1(X_i) = \frac{1}{(N-1) \cdot \rho_N(i)}, \quad \hat{P}_0(X_i) = \frac{1}{M \cdot v_M(i)} \tag{3.15}$$

Here k is set to be 1 because it has been shown that the divergence estimator is still consistent when sample size goes to infinity with $k = 1$, even though the density estimates

are not. Therefore, from (3.11) (3.14) and (3.15), we have

$$\begin{aligned} D(P_1\|P_0) &= \frac{1}{N}\sum_{i=t_{te}}^{t}\log\frac{\frac{1}{(N-1)\cdot\rho_N(i)}}{\frac{1}{M\cdot v_M(i)}} \\ &= \frac{1}{N}\sum_{i=t_{te}}^{t}\log\frac{v_M(i)}{\rho_N(i)} + \log\frac{M}{N-1} \end{aligned} \tag{3.16}$$

$$\boldsymbol{\lambda}(t) = \sum_{i=t_{te}}^{t}\log\frac{v_M(i)}{\rho_N(i)} + N\cdot\log\frac{M}{N-1} \tag{3.17}$$

This estimator proves to be asymptotically unbiased and mean-square consistent. However, it may not be very suitable for change detection, as we will figure out in Section 3.5.

3.3.2 Optimization Approach: KLIEP

Another way to estimate the probability density ratio $\boldsymbol{\lambda}$ is the KLIEP originally proposed in [36]. It approximates the density ratio $w(x)$ by minimizing the K-L divergence from the true density $f_1(x)$ to its estimate $\hat{f}_1(x)$ in (3.18), which should be 0 if the estimate is the same as the true one:

$$\hat{f}_1(x) = \hat{w}(x)f_0(x). \tag{3.18}$$

The K-L importance $w(x)$ is defined as the density ratio between $f_1(x)$ and $f_0(x)$ at x. The core of this algorithm is to approximate the importance $w(x)$ with coefficients α and kernels ϕ as in (3.19), and minimize the divergence between $\boldsymbol{X}_{te}$ and $\hat{\boldsymbol{X}}_{te}$ over different $\vec{\alpha}$ and $\vec{\phi}$. According to the expression of K-L divergence given in (3.10) and (3.11), we have

$$\hat{w}(\boldsymbol{X}) = \sum_{l=1}^{L}\alpha_l\cdot\phi_l(\boldsymbol{X}), \tag{3.19}$$

$$\begin{aligned} D(P_1\|\hat{P}_1) &= \frac{1}{N}\sum_{x\in\boldsymbol{X}_{te}}\log\frac{P_1(x)}{P_0(x)\cdot\hat{w}(x)} \\ &= \frac{1}{N}\sum_{x\in\boldsymbol{X}_{te}}\log\frac{P_1(x)}{P_0(x)} - \frac{1}{N}\sum_{x\in\boldsymbol{X}_{te}}\log\hat{w}(x). \end{aligned} \tag{3.20}$$

The optimization problem can be written as (3.21) because the first term in (3.20) has nothing to do with $\hat{w}(x)$:

$$\min D(P_1 \| \hat{P}_1) \Longleftrightarrow \max \sum_{x \in \boldsymbol{X}_{te}} \log \hat{w}(x). \tag{3.21}$$

The optimization constraint can be given by (3.22) because of the normalization requirement of $\hat{P}_1$:

$$1 = \int \hat{w}(x) P_0(x) dx = \frac{1}{M} \sum_{x \in \boldsymbol{X}_{tr}} \sum_{l=1}^{L} \alpha_l \cdot \phi_l(x). \tag{3.22}$$

The optimization above is concave; thus the global optimum can be reached with methods such as gradient ascent. After we attain the solution $\hat{w}(x)$, we can compute the $\boldsymbol{\lambda}$ by using

$$\boldsymbol{\lambda} = \sum_{x \in \boldsymbol{X}_{te}} \log \hat{w}(x). \tag{3.23}$$

The choice of kernel or basis functions in this optimization is important. In [11], a non-parametric KLIEP paired with Gaussian kernel centered at testing data is adopted for sequential detection, and the model selection is carried out by likelihood cross validation (CV):

$$\begin{aligned} \hat{w}(\boldsymbol{x}) &= \sum_{l=1}^{N} \alpha_l \cdot K_\sigma(x, \boldsymbol{X}_{te}(l)) \\ &= \sum_{l=1}^{N} \alpha_l \cdot exp(-\frac{\|x - \boldsymbol{X}_{te}(l)\|^2}{2\sigma^2}). \end{aligned} \tag{3.24}$$

It has been shown that [36] when a non-parametric model (e.g., kernel basis functions centered at test samples) is adopted for the importance estimation, KLIEP converges to the optimal value with a rate slightly slower than $\mathcal{O}(n^{-1/2})$ under $n = N = M$, where N (M) is the size of X_{te} (X_{tr}). Thus we keep the testing data size the same as that of the training data in this algorithm for the rest of this chapter.

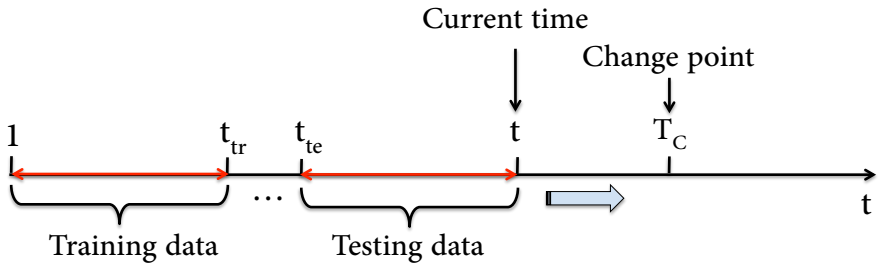

Figure 3.1: Change detection scenario

3.3.3 Change Detection

The aforementioned two approaches both work well in estimating the importance or density ratio between two distributions. It's been shown that both are asymptotically unbiased and consistent. However, the nearest neighbor approach has a larger variance than KLIEP at small sample size[42]. So we mainly focus on change detection based on KLIEP.

We directly apply KLIEP to the detection problem by moving the testing data window forward when new data come in, while keeping the training data window fixed, as in Fig. 3.1.

When $t > T_C$, data samples subject to F_1 fall in the testing window, and the value of $\boldsymbol{\lambda}(t)$ will increase. H_1 in (3.5) is claimed true when $\boldsymbol{\lambda}(t)$ hits some threshold Γ at time τ, which means that the change point is detected.

In fact, this straightforward non-parametric detection has been used in [36]. We hereby give KLIEP based change detection in Algorithm 3.

Algorithm 3 works in detecting the change. However, it can be further improved using the concept of CUSUM, by exploiting the historical data, we have

$$\begin{aligned} \tau^* &= \inf\{t \geq 1 : \max_{1 \leq t_{te} \leq t} \sum_{i=t_{te}}^{t} l(X_i) \geq \gamma\} \\ &= \inf\{t \geq 1 : \max_{1 \leq t_{te} \leq t} \boldsymbol{\lambda}_{t_{te}}(t) \geq \gamma\}. \end{aligned} \tag{3.25}$$

Algorithm 3: Change detection based on KLIEP

Input: Data samples X_i, $i = 1, 2, \cdots, t$. t is the current time; N as the training/testing window size; T as the threshold

Output: τ: time when a change is claimed

Initialization:

$$t_{te} \leftarrow N+1 \quad t \leftarrow 2N$$
$$\lambda \leftarrow 0 \qquad \boldsymbol{X}_{tr} \leftarrow \boldsymbol{X}_i, i \in [1, N]$$

while $\lambda \leq T$ **do**
- $X_{te} \leftarrow X_i, i \in [t_{te}, t]$
- $\lambda = f_{KLIEP}(\boldsymbol{X}_{tr}, \boldsymbol{X}_{te})$
- **if** $\lambda \geq T$ **then**
  - $\tau \leftarrow t$ and **break**
  - **else**
    - $t \leftarrow t+1$, $t_{te} \leftarrow t_{te}+1$

return τ

However, since we don't have the prior information to compute the LR at each time, we propose a truncated version of (3.25), which is given by

$$\hat{\tau}^* = \inf\{t \geq t_0 : \max_{w_{lo} \leq t_{te} \leq w_{up}} \boldsymbol{\lambda}_{t_{te}}(t) \geq \gamma\}, \tag{3.26}$$

and

$$\begin{aligned} w_{lo} &= \max\{t-N-W+2, N+W+1\} \\ w_{up} &= t-N+1, \quad t_0 = 2N+W \end{aligned}, \tag{3.27}$$

where N is the minimum length of training/testing data $\boldsymbol{X_{te}}$ and $\boldsymbol{X_{tr}}$, and W is the truncated window size in window truncated CUSUM quickest detection in Algorithm 4.

This proposed algorithm maintains W testing data windows corresponding to $\boldsymbol{\lambda}_{t_{te}}$ in (3.26), where $w_{lo} \leq t_{te} \leq w_{up}$. Then we compare the maximum of these $\boldsymbol{\lambda}$ with the threshold γ. If at time t, the maximum hits γ, we claim the change time or stopping time $\tau^* = t$. The window size W should be selected properly, which is closely related to the computational complexity. The choice of threshold and window size will be discussed in the next section.

Algorithm 4: Window truncated change detection based on KLIEP

Input: Data samples X_i, $i = 1, 2, \cdots, t$. t is the current time; N as the minimum training/testing data size; W as the truncated window size; γ as the threshold

Output: τ: time when a change is claimed

Initialization:

$$t_{te} \leftarrow t_0 - N + 1 \quad t \leftarrow t_0$$
$$\lambda \leftarrow 0 \qquad \boldsymbol{X}_{tr} \leftarrow \boldsymbol{X}_i, i \in [1, N]$$

while $\lambda \leq \gamma$ **do**
  for $k = 1 : W$ **do**
    $\boldsymbol{X}_{te} \leftarrow \boldsymbol{X}_i, i \in [t_{te} - (k-1), t]$
    $\boldsymbol{X}_{tr} \leftarrow \boldsymbol{X}_i, i \in [1, N + (k-1)]$
    $\lambda_k = f_{KLIEP}(\boldsymbol{X}_{tr}, \boldsymbol{X}_{te})$
  $\lambda_{max} = \max\{\lambda_1, \lambda_2, \cdots, \lambda_k\}$
  if $\lambda_{max} \geq \gamma$ **then**
    $\tau \leftarrow t$ and **break**
    else
      $t \leftarrow t + 1$, $t_{te} \leftarrow t_{te} + 1$

return τ

3.4 Performance Analysis

Our proposed window-truncated K-L importance based change detection is modified based on the traditional CUSUM test. Compared with the CUSUM stopping time τ^* defined in (3.4), our stopping time $\hat{\tau}^*$ defined in (3.25) has a truncated window with upper limit w_{up} and lower limit w_{lo} instead of from $t = 1$ to the current time. Furthermore, the sum $\sum l(X_i)$ is estimated with KLIEP algorithm, which is purely data driven, thus not being error-free.

It is very difficult to analyze the detection performance with estimation error. Though it has been proved asymptotically optimal under certain conditions, in our case, with only limited testing and training data, the convergence is definitely not guaranteed. However, from numerical results, we can assume that it is almost correct. Hence, in this section we will analyze the window-truncated quickest detection assuming that the estimation is correct.

In standard CUSUM quickest detection, the CUSUM stopping time as in (3.25) is shown to achieve the minimum detection delay given a false alarm constraint. To analyze the performance of the quickest detection, we first define two average run lengths (ARLs) [28] as the metrics, which are also widely used as the performance criteria in many other studies

[24, 10]. These two ARLs are given by $E_0\tau^*$ and $E_1\tau^*$, where E_0 and E_1 are the expectations under P_0 and P_1 respectively. Then, we define the worse case delay $\bar{E}_1\tau^*$ as

$$\bar{E}_1\tau^* = \sup_{t\geq 1} ess\sup E^{(t)}[(\tau^* - t + 1)^+ | \mathcal{F}_{t-1}]. \tag{3.28}$$

Therefore by the definition, we can observe that $E_0\tau^*$ represents the average time before we make a false alarm (namely claiming that there is a change while nothing happens), and that $E_1\tau^*$ stands for the detection delay with stopping time τ^*.

Now let us come back to our problem formulated in Section 3.2. We hope that our detection algorithm can minimize the worst-case delay $D_W(\tau^*) = \bar{E}_1\tau^*$ given the false alarm constraint $P_{FA} \leq \alpha$. We define $\eta = \frac{1}{\alpha}$ which corresponds to the ARL $E_0\tau^*$. Then the constraint $P_{FA} \leq \alpha$ is equivalent to the ARL constraint $E_0\tau^* \geq \eta$

Due to Theorem 1 in [14], the baseline ARL constraint can be replaced with

$$\sup_{T_C\geq 1} P_0(T_C \leq \tau^* < T_C + W(\alpha)) \leq \alpha, \tag{3.29}$$

where $W(\alpha)$ is a positive integer only related to α satisfying

$$\liminf W(\alpha)/|\log\alpha| > I^{-1}, \tag{3.30}$$

$$\log W(\alpha) = o(\log\alpha), \tag{3.31}$$

where I is the K-L divergence defined in (3.8) given i.i.d. X_i.

$$\begin{aligned} &P_0(t \leq \tau^* < t + W(\alpha)) \\ &\leq \sum_{n=t}^{t+W(\alpha)-1} P_0\left(\prod_{i=n-k}^{n} \frac{f_1(X_i)}{f_0(X_i)} \geq e^\gamma \text{ for some } k \leq n-1\right) \end{aligned} \tag{3.32}$$

Because under P_0, $X_n, X_{n-1}, \cdots, X_n$ has the same distribution as $X_1, X_2, \cdots, X_n$, we can further have

$$\begin{aligned} &\leq W(\alpha) P_0\left(\prod_{i=n-k}^{n} \frac{f_1(X_i)}{f_0(X_i)} \geq e^\gamma \text{ for some } t \geq 1\right) \\ &\leq W(\alpha) e^{-\gamma}. \end{aligned} \tag{3.33}$$

The last step in (3.33) uses the Doob's submartingale inequality. Comparing this with (3.29), we have

$$W(\alpha)e^{-\gamma} \leq \alpha. \tag{3.34}$$

Then by Theorem 4 in [14], it is shown that the window-limited stopping rule, given by

$$\bar{\tau}^* = \inf\{t : \max_{t-W+1 \leq t_{te} \leq t} \sum_{i=t_{te}}^{t} l(X_i) \geq \gamma\}, \tag{3.35}$$

can achieve the same uniform asymptotic lower bound of detection delay as in (3.37) with properly chosen threshold γ and window length W, satisfying

$$2W(\alpha)e^{-\gamma} = \alpha, \tag{3.36}$$

$$E^{(T_C)}(\bar{\tau}^* - T_C)^+ \sim \frac{P_0(\bar{\tau}^* \geq T_C)|\log \alpha|}{I} \quad as\ \alpha \to 0. \tag{3.37}$$

The worst-case delay $E_1(\bar{\tau^*})$ is upper bounded by $\frac{\gamma}{I}$, as $\gamma \sim |\log \alpha| \to \infty$, i.e. $\alpha \to 0$. However, due to the limitation on K-L importance estimation procedure, we can't estimate it based on too few observations. Thus we set a minimum training/testing data size N, and modify the $\bar{\tau}^*$ to $\hat{\tau}^*$ by changing the lower bound from $t - W + 1$ to $t - W - N + 2$ and the upper bound from t to $t - N + 1$, as defined in (3.26). This is a tradeoff between the estimation and detection precision. When N is small, the stopping time $\hat{\tau}^*$ is more like $\bar{\tau}^*$ which is shown to be asymptotically optimal given properly selected threshold and window size W, whereas the estimation variance and error may be larger than that when N is large; and vice versa. Since we have no prior information on F_0 and F_1, we don't know the true divergence I either; hence we could not decide the proper W based on (3.30). However, given certain conventional false alarm rate lower bound α, we can set parameters for the worst case, where the divergence I is a very small value. The resulting threshold γ can be very large to guarantee the false alarm rate.

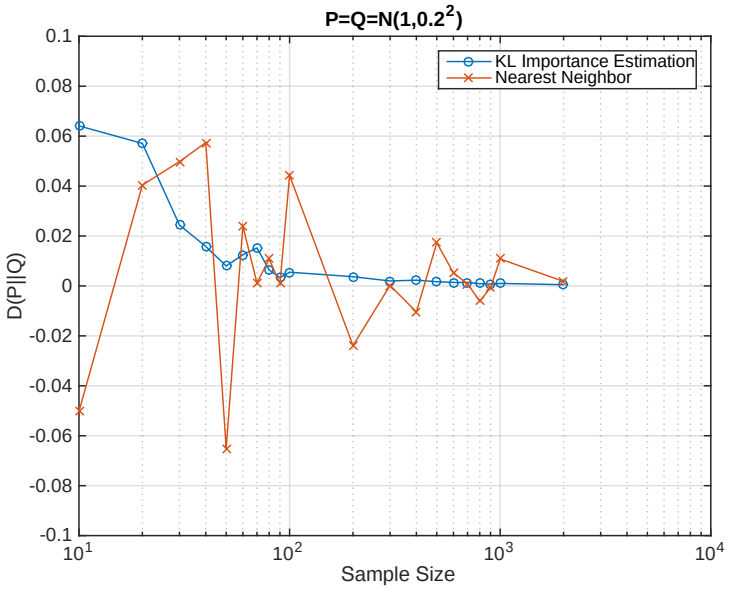

Figure 3.2: Estimation of divergence between the same distribution

3.5 Numerical Results

In this section, we use numerical simulation results to demonstrate the performance of our proposed importance estimation based quickest sensing. Firstly, as mentioned in Section 3.3, we don't adopt the nearest neighbor approach in our proposed non-parametric quickest detection for spectrum sensing. Though the estimator is shown to be unbiased and mean-square consistent, its not very reliable with finite samples. When the divergence to estimate is 0, i.e. $P_0 = P_1$, the nearest neighbor estimator has large variance as can be seen in Fig. 3.2. Thus before the change (PU's presence) actually occurs, the estimated divergence $D(P_0\|P_1)$ or the sum of log-LR λ can be largely deviated from 0, compared to KLIEP approach.

We tested our proposed KLIEP-based approach, the universal quickest spectrum sensing algorithm, with some random chosen F_0 and F_1, as is modeled in (3.1). We choose window size $W = 5$ and testing data size $N = 25$ for all tests. In Fig. 3.3, we show two scenarios when the pre-change and post-change distributions are Gaussian, most commonly.

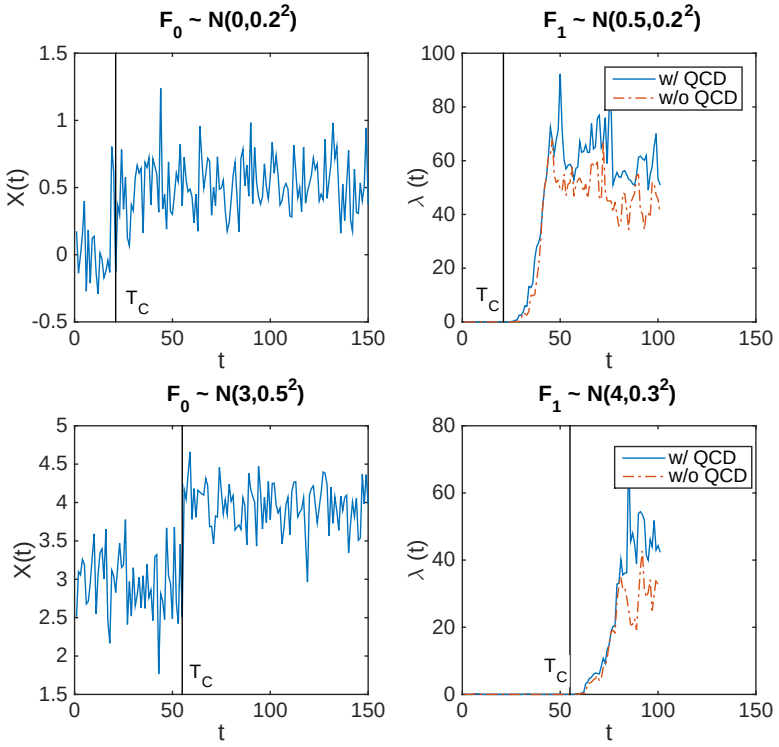

Figure 3.3: Change detection: Gaussian to Gaussian case

In Fig. 3.4, we show two non-Gaussian scenarios where pre and post change distribution can be Gaussian, Laplacian or Uniform, etc. The vertical line marks the change point T_C. We can see that the proposed quickest detection method reacts to the change quicker than the traditional KLIEP detection, regardless what type of distribution and parameters that F_0, F_1 are subject to. By setting different thresholds γ, we can obtain the Receiver Operating Characteristic (ROC) curve for any setting, which gives average detection delay $E_1\hat{\tau}^*$ to different false alarm rate $1/E_0\hat{\tau}^*$. We show two ROC curves at the setting of $F_0 \sim N(0, 0.2^2)$ and $F_1 \sim N(0.4, 0.3^2)$, where the divergence between the pre-change and post-change distributions is 2.22, and $F_0 \sim N(0, 0.2^2)$ and $F_1 \sim N(0.2, 0.3^2)$, where the divergence is 0.72, as given in Fig. 3.5. It can be seen that our proposed quickest sensing outperforms the traditional KLIEP sequential detection, at the cost of extra computational cost.

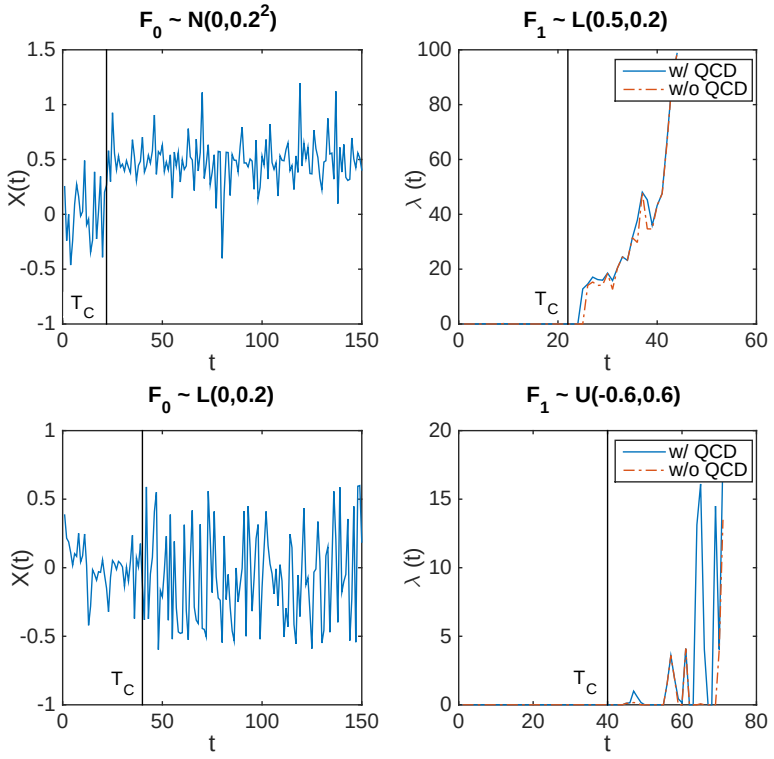

Figure 3.4: Change detection: non-Gaussian case

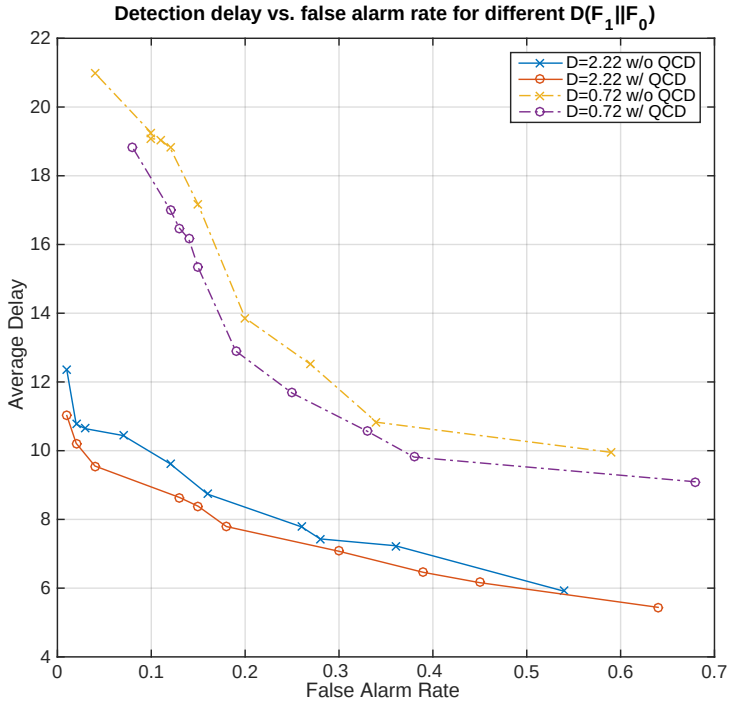

Figure 3.5: ROC curve for certain pre and post change distributions

3.6 Conclusion

In this chapter we've proposed a spectrum sensing technique, which is essentially a non-parametric quickest change detection, based on K-L importance estimation and CUSUM test. With the proposed algorithm, quickest spectrum sensing can be carried out without any prior knowledge of F_0 and F_1, thus being universal. The sensing performance measured by detection delay vs. false alarm rate is shown to be better than traditional KLIEP based non-parametric sequential detection. However, a tradeoff has to be made between the increased computational cost and better sensing performance.

In our future work we'll improve the threshold selection, which can adaptively adjust the threshold to the sensing process. We'll also try to lower the computational cost for SUs by exploiting the historical optimization coefficients to update the current estimation instead of going through the whole optimization process at each time.

Chapter 4

Universal Quickest Sensing of Spectrum Change in Millimeter Wave Communications: A Data Driven Approach

This chapter is revised based on a conference paper by Yifan Wang, Zhiyang Zhang and Dr. Husheng Li:

Wang, Y., Zhang, Z., & Li, H. (2017). Universal Quickest Sensing of Spectrum Change in Millimeter Wave Communications: A Data Driven Approach. In *2017 IEEE Global Communications Conference (GLOBECOM)* (pp. 1-6). IEEE.

Abstract

As millimeter wave is becoming the fundamental signaling technology of the physical layer standard in the next generation cellular network, it also brings about many questions and challenges. Not all the existing theories and methods for traditional wireless communications can apply directly to millimeter wave network because of the adoption of directional antenna, blockage effect, and the unprecedentedly large bandwidth. Among them, spectrum sensing is one of the open challenges, for the purpose of dynamic spectrum access in the millimeter wave band. In this chapter, we propose a data driven sensing technique based on the mean recurrence time of random process to efficiently detect the change in the primary user (PU) activities, which can tolerate small fluctuations in the distribution. The proposed spectrum sensing works well without a priori knowledge of the PUs, and does not take the assumption of independent and identically distributed observations on the PUs. It can also serve as a general framework for change detection in other areas.

4.1 Introduction

Compared with traditional wireless communications such as 2.4 GHz Wi-Fi networks and 4G cellular networks, millimeter wave (mmWave) communications, as its name suggests, works in a much shorter wavelength in millimeter scale. Since a shorter wavelength means higher frequency, mmWave corresponds to the frequency band between 30 GHz to 300 GHz. During the past decades, thorough researches on traditional cellular wireless communication have been conducted. Though physics and the characteristics of mmWave have been theoretically studied extensively, only until recent few years, were mmWave bands considered

and implemented in practical communication systems [31], such as IEEE 802.15. 3c [1] and IEEE 802.11 ad [30].

The motivation of adopting mmWave is obvious: crowded frequency spectrum and huge demand in transmission rate. By moving wireless signals to a higher frequency band, it alleviates the congestion of data traffic in lower frequency bands. In addition, whereas the current cellular networks support the data rate of hundreds Megabits-per-second (Mbps), the next generation (5G) cellular networks that adopt mmWave as the physical (PHY) layer standard can increase the peak data rates to gigabits-per-second (Gbps).

However, along with the advantages of mmWave, there are many limitations for the high speed data transmissions such as limited non-line-of-sight (NLOS) signal range [22]. Despite the potential usage of this limitation like object tracking [48][49], in terms of wireless communication, challenges are that some traditional theories and techniques could not apply directly to the mmWave scenario. One most important factor that causes this challenge is the employment of steerable directional antennas at communication nodes and base stations, which makes communication links isolated directionally, with interference playing a less important part than in current cellular networks.

In mmWave networks, we do have abundant spectrum resource and directional antennas. However, as the Internet of Things (IoT) rapidly grows [45], scenarios in which multiple nodes co-existing in small cells need to communicate with each other in the same frequency will become more and more common. Therefore dynamic spectrum access with spectrum sensing may be needed to avoid interference and schedule the resource in a more efficient manner in the future mmWave networks. Meanwhile, in military communications, spectrum sensing is always useful, not only for saving the spectrum resource but also for swiftly detecting primary user (PU)'s activities and finding available spectrum bands.

Spectrum sensing is known as a key to higher spectrum efficiency, where secondary users (SU) without license to the frequency band (which is licensed to PUs) can use this band to communicate with each other, when PUs are silent. Essentially, SUs can only use the spectrum when their communications do not interfere with PUs. Therefore in the scenario of mmWave cognitive radio networks, the presence of PUs does not necessarily mean a short distance between the PU and SUs due to the directionality of mmWave antennas; instead

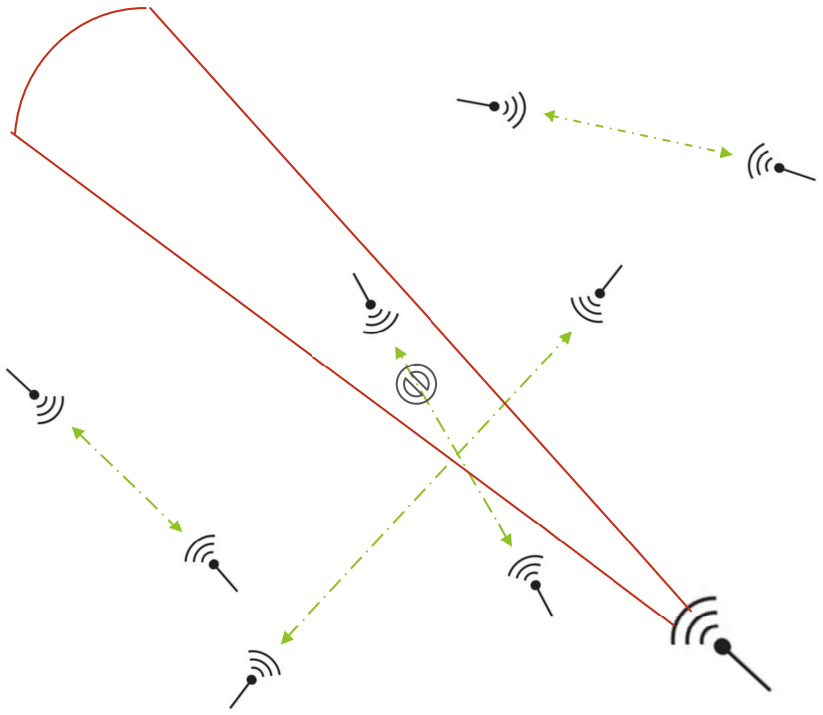

Figure 4.1: mmWave cognitive network with a PU and SUs

it means that an SU can determine that PU's transmission energy is above some limit. Due to the advantage of directional antennas, an SU near a PU can still communicate with other SUs with beam adaptation in the licensed band as long as it is not transmitting in the direction of the PU. Another difference is that mmWave signal suffers from a more severe non-line-of-sight loss than traditional networks. Therefore the sensed signals are more vulnerable to the environmental changes. Compared with traditional communications, where the spectrum sensing can usually be modeled as a ON-OFF change detection problem, and can be solved using the likelihood ratio approach such as the cumulative sum (CUSUM) test, in mmWave communications, there can be some small distribution changes that are caused by the environmental fluctuation and antenna leakage, which can be tolerable for SUs. Hence, the SUs only need to detect more significant changes indicating the presence of PUs. Fig. 4.1 shows a cognitive network where a PU and several SUs with directional antennas are within the same area.

Hence, we cannot directly apply existing spectrum sensing techniques to detect the spectrum change of PUs in mmWave Cognitive networks. To our best knowledge, there

are few studies on mmWave spectrum sensing where no assumption of independent and identically distributed (i.i.d.) observations on the PUs is made. In this chapter we propose a universal mmWave spectrum sensing technique based on the mean recurrence time (MRT) of random process [33], which does not assume the distributions before and after the change points and not assume independence of the underlying random variables of the sensed signal. Though the proposed method is based on the signal strength or energy detection, it can also serve as a framework for change detection in any other metrics, such as phase, frequency, etc.

The remainder of this chapter is organized as follows. In Section 4.2 the system model is provided. In Section 4.3, which is the main technical part of this chapter, we propose a universal mmWave spectrum sensing approach for change detection in the mmWave band. Then numerical results based on real mmWave measurements are shown in Section 4.4, while some theoretical performance analysis is given in Sction 4.5. Finally Section 4.6 concludes the chapter.

4.2 System Model

In this chapter, all the transceivers (PUs and SUs) are mmWave zero-intermediate-frequency (IF) ones [38] equipped with directional antennas. An SU in the network directly down-converts to the base band whatever it received, and regards it as the sensed signal. Such a baseband sensing avoids the necessity of direct sampling in the mmWave band. When the PU's transmission direction points to an SU at some time, the sensed energy at this SU will significantly increase due to the focused power. Then the SU will claim that the PU turns ON if a threshold is hit, thus stopping its data transmission to avoid interfering the PU. Similarly, when the sensed energy experiences an abrupt decrease, which is usually caused either by the change of the PU's transmission direction or the decreasing distance between SU and PU or a temporary blockage, the impacted SU will claim that the PU status goes OFF, and start transmitting.

We model the spectrum sensing at an SU as a change detection problem. Without the loss of generality, we denote by X_t the sensed signal power at an SU that is in the absence

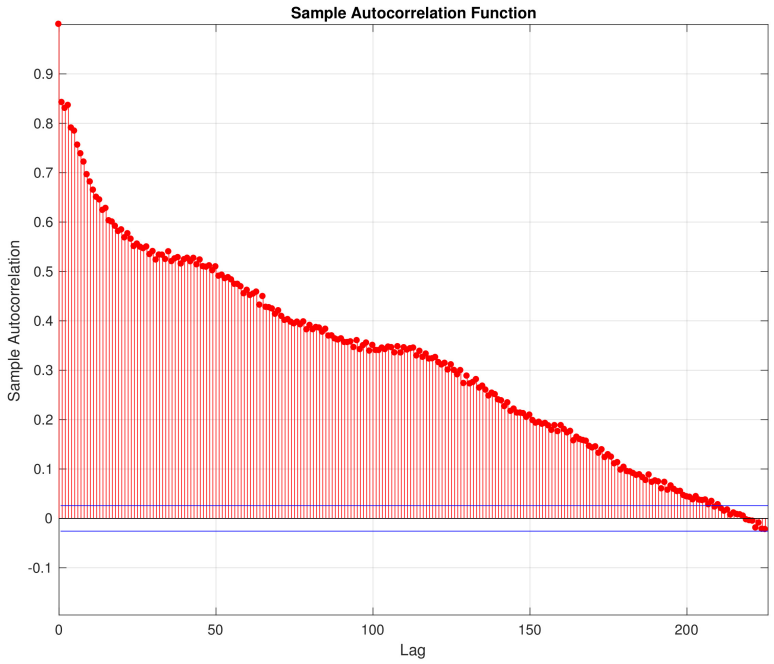

Figure 4.2: Sample autocorrelation of the sensed signal

of PU and by Y_t in the presence of PU. The random process of sensing observation is given $Z = \{X_1, X_2, \ldots, X_{T-1}, Y_T, Y_{T+1}, \ldots, \}$, which stands for the sensed signal energy at an SU, when the PU's status changes from OFF to ON at time T. At the change time T, the PU starts transmitting in the direction of the SU's antenna, which results in the significant change in the random process Z (from X to Y). We have the following hypothesis testing:

$$\begin{cases} H_0 : Z \sim X \\ H_1 : Z \sim Y \end{cases} \tag{4.1}$$

The same modeling can also be applied to detect the change from Y (active PU) to X (inactive PU). In the subsequently proposed algorithm, the detection is carried out regardless of X to Y or Y to X. Notice that X_t may not necessarily be an i.i.d. process; neither is Y_t. Therefore the likelihood ratio based change detection such as CUSUM test may not work well. The reason we do not make the i.i.d. assumption is based on the real measurement of sensed signals in the mmWave band (the measurement setup will be elaborated in Section 4.4), which can be illustrated by the sample autocorrelation of the signal shown in Fig. 4.2.

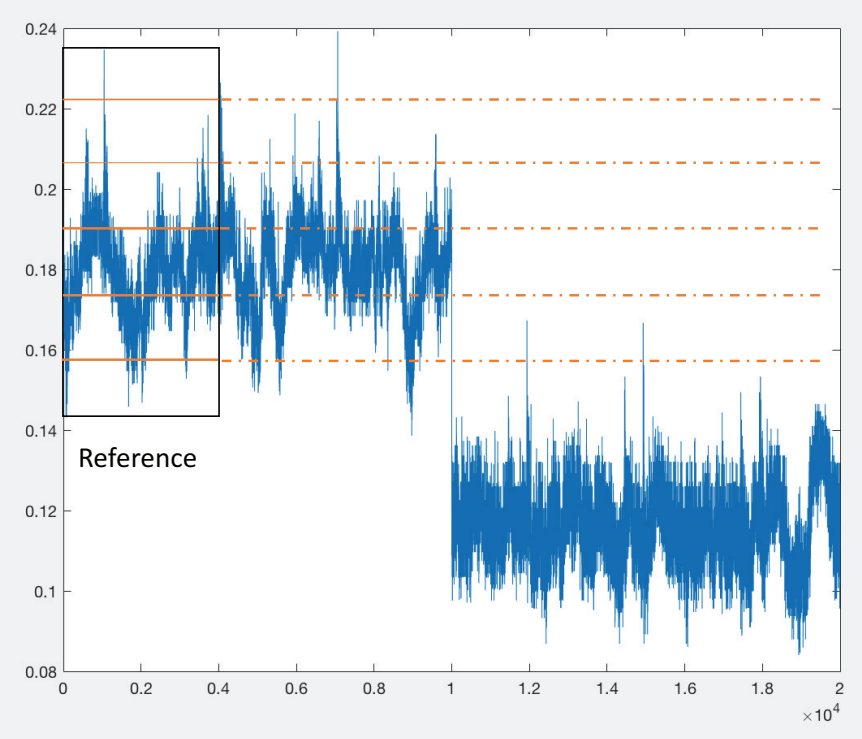

Figure 4.3: Example of sensed signal and quantization

We then model the random process $\{X_t, t = 1, 2, 3, \ldots, K\}$ as a discrete finite state Markov chain by uniformly quantizing the variables X_t into P states based on their values. The full scale range (FSR) depends on the minimum and maximum of the first K variables as shown in figure 4.3, and K is the length of the reference samples:

$$\begin{aligned} Q_{min} &= \min\left(X_1, X_2, \ldots, X_K\right) \\ Q_{max} &= \max\left(X_1, X_2, \ldots, X_K\right) \end{aligned} \tag{4.2}$$

Any sample that falls outside the interval $[Q_{min},\ Q_{max}]$ will be assigned to the boundary state 1 and P accordingly. We assume the ergodicity and stationarity of the random process Z before the change time T such that at all the states have bounded MRT (the definitions of recurrence and MRT are given in the Appendix F). It is intuitive to believe that if the "structure" of the random process Z significantly changes at time T due to the change of PU's activities, a portion of the states will not be revisited or at least not as that frequently as before time T, namely no longer recurrent.

Inspired by this idea, we hereby adopt MRT as the criterion for decision making. If the MRT of a certain number of states becomes too large or in the extreme case, infinite which means the states are not recurrent after T, the SU can claim a change as the sensing result.

4.3 Universal Spectrum Change Sensing

For each SU, the purpose of spectrum change sensing is to avoid interfering with the PU and capture the spectrum opportunity. Normally, we consider these following scenarios of possible interference:

- An SU's antenna points to the PU and the PU transmits in the direction of this SU.
- Similarly to the first scenario, but the SU is transmitting in the direction of PU after reflections.
- PU and SU are not exactly pointing to each other, but with some small angle deviation.
- The PU is on the transmission path of an SU, but the PU's antennas are not pointing to the SU.

Except for the first scenario, where the SU's transmission could directly impact the PU, the interference level varies depending on the attenuations resulting from reflections and angle of incidence. In the second scenario the interference level depends on the channel loss and fading due to the reflection; in the third and fourth cases, it depends on the antenna radiation pattern such as the main lobe width and side lobe level.

In the previous section, we point out in the system model that no assumption of the pre-change or post-change distributions is made. Without the loss of generality, we take H_0 as the "PU is absent" and H_1 as "PU is present". Hence, in the hypothesis testing (4.1), we have

$$X = w, \quad Y = w + S, \tag{4.3}$$

where w is the random noise process, and S is the random process of the sensed signal energy, which depends on the SU antenna pattern, PU transmission power, PU antenna gain, the angle of incidence, etc. Since w and S are not subject to certain known distributions, we

cannot take advantage of the likelihood ratio based detection algorithm, such as CUSUM quickest detection [28]. Even the data-driven quickest detection with i.i.d. assumption in our previous work [43] cannot apply, since the estimated divergence is always high and undesired spikes will result in a high false alarm rate.

Therefore by exploiting the concept of MRT, an SU could tell if there is a drastic change in the statistics of sensing signals, as mentioned in Section 4.2. First, the SU quantizes the reference sensed signal, which is assumed to be subject to H_0, into P states. Then it calculates the MRT for each of the P state. Instead of calculating the MRT by using the following definition:

$$T_i^{MRT} = E[T_i] = \sum_{t=1}^{+\infty} t f_{ii}(t) \tag{4.4}$$

where $f_{ii}(t)$ stands for the probability that it revisits state i from state i after t steps, an SU can estimate $E[T_i]$ and $Var[T_i]$ numerically based on the reference data, since SUs do not know the exact transition probabilities of the Markov chain. Then, the SU claims a change when a certain fraction of states have not been revisited long enough, which is controlled by two parameters, the fraction ϵ and the threshold coefficient β. Denoting by τ_i the time elapsed since the last visit to the state i, we have the following decision rule:

$$\tau_i \geq E[T_i] + \beta\sqrt{Var[T_i]} \tag{4.5}$$

$$\frac{1}{P}\sum_{i=1}^{P} 1_{\tau_i \geq E[T_i]+\beta\sqrt{Var[T_i]}} > \epsilon \tag{4.6}$$

Remember that we only consider significant changes; hence, the observation $S + w$ must have several states that do not frequently appear in w, and w must also have several states that are not frequently revisited any longer in $S + w$. We can adjust the sensitivity of the sensing by controlling the value of β and ϵ.

Algorithm 5: Mean-recurrence-time detection

Input: Reference samples $\mathbf{X}_r = \{X_1, X_2, \cdots, X_K\}$, sensed input $X_t, \{t = t_0, t_0 + 1, \cdots\}$, quantization step P, threshold coefficient β, fraction ϵ

Output: $\mathcal{T}$

Initialization: $\forall i \in [1, P]$ $\tau_i = 0, t = t_0$

Quantize $\mathbf{X}_r : Q(\mathbf{X}_r) = \{Q(X_1), Q(X_2), \cdots, Q(X_K)\}$

Estimate $E[T_i]$ and $Var[T_i]$ $\forall i \in [1, P]$ based on $Q(\mathbf{X}_r)$

while $\frac{1}{P}\sum_{i=1}^{P} 1_{\tau_i \geq E[T_i]+\beta\sqrt{Var[T_i]}} < \epsilon$ **do**

  Quantize $X_t : Q(X_t) = j$, $j \in [1, P]$

  $\tau_i \leftarrow \tau_i + 1, \forall i \in [1, P] \setminus j$

  $\tau_j \leftarrow 0$

  $t \leftarrow t + 1$

$\mathcal{T} \leftarrow t$

return $\mathcal{T}$

4.4 Experiment and Numerical Results

In this section, we show the experiment and numerical results based on real mmWave measurement.

4.4.1 Experiment Setup

All our experiments are based on the measured data of our mmWave testbed, whose components are listed in Table 4.1.

Table 4.1: Experimental hardware and software

Input	Tektronix AFG3102C
External Clock	Tektronix TSG4102A
TX	Motherboard with the TX module HMC6300
RX	Motherboard with the RX module HMC6301
Software	HMC6300/HMC6301 Graphical User Interface
Oscilloscope	Tektronix DPO 70404C

The system board used in our experiment is Analog Devices EK1HMC6350 evaluation kit as is shown in Fig. 4.4a, which allows us to set up a half-duplex, 60 GHz millimeter wave link using standard baseband analog interfaces. And the daughter board HMC6301 as the receiver is pictured in Fig. 4.4b while the transmitter HMC6300 in Fig. 4.4c.

In our experiment, the zero IF transmitter (PU) directly up-converts the base band signal to the carrier frequency which is set to be 56.5 GHz on the EK1HMC6350 board. We use 1 MHz sinusoid as the base band signal for simplicity because energy detection does not have much to do with the data content. On the SU side, it directly down-converts the received mmWave signal to zero IF with the synchronized oscillators (LO). We also fix the receiver's gain such that the SU needs no further calculations to compare the sensed signal strength with and without PU's presence.

The antennas in the picture are pyramidal horn antennas which has the pattern given in Fig. 4.5.

Due to the hardware limit, we only carry out experiment using one pair of transceivers with different parameters. To focus on the problem of change detection, we adopt the same LO to eliminate the frequency deviation between the transmitter and receiver. We simulate the scenarios of "PU is present" and "PU is absent" by changing the distance between PU and SU or the angle of incidence on SU's antennas. Longer distance or larger angle deviation of incidence means more signal attenuation.

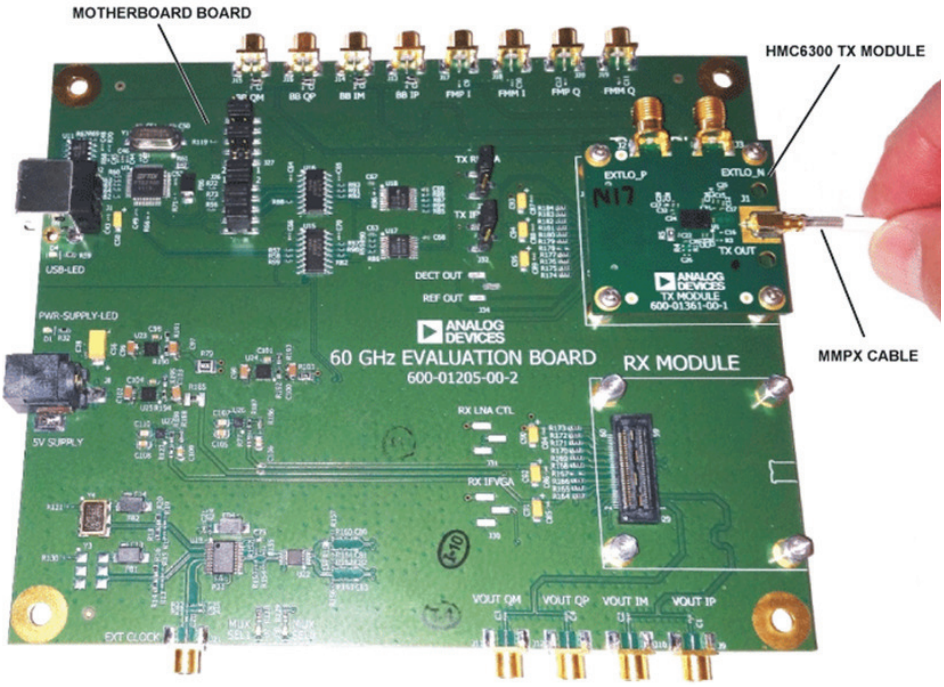

(a) 60 GHz evaluation board

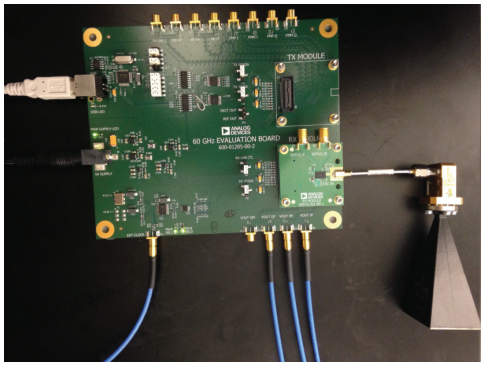

(b) Motherboard with RX Module

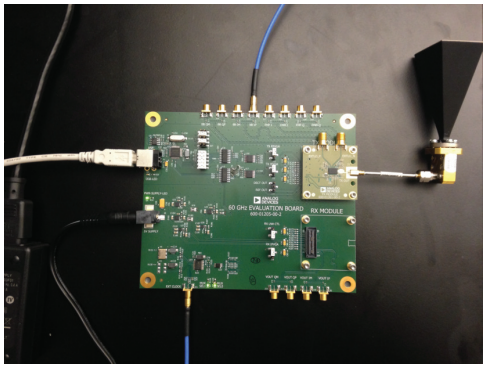

(c) Motherboard with TX Module

Figure 4.4: Experiment hardware : motherboard, RX module HMC6301 and TX module HMC6300 with USB, DC power, Horn Antenna, external clock and I/Q cables installed

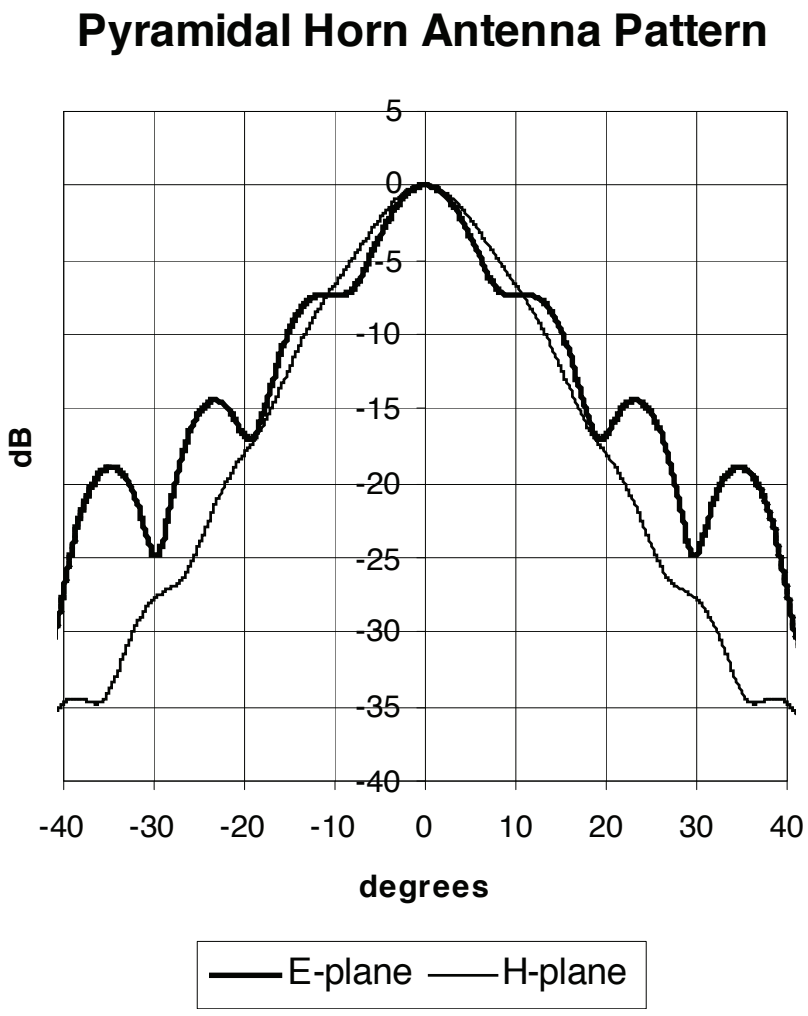

Figure 4.5: The adopted antenna pattern

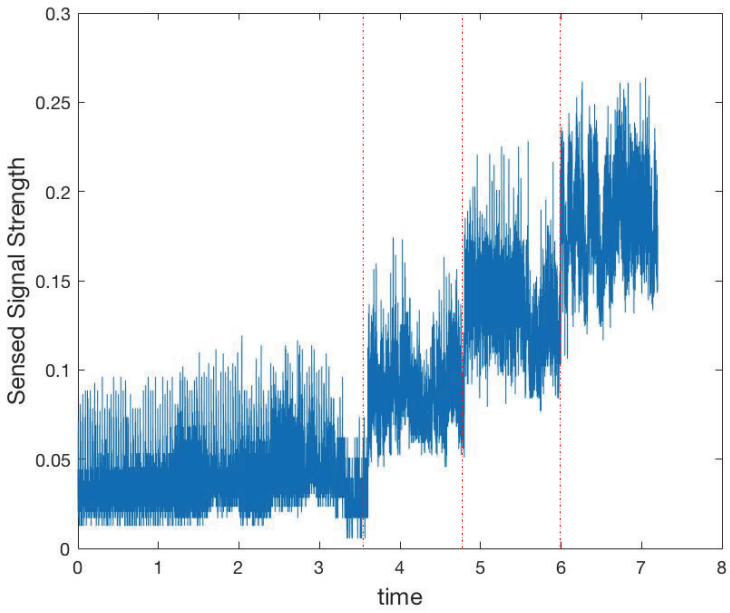

Figure 4.6: Sensing signals for different angles of incidence

Fig. 4.6 illustrates the sensed signal power over different angles of incidence, where after $t = 6$ the angle of incidence on the SU's antenna is $0°$ indicating that PU is transmitting directly towards SU's antenna.

4.4.2 Numerical Results

We tested the sensing performance in terms of average delay and false alarm rate, which is the number of false alarms out of all tests, based on 1000 runs. In each test, we randomly choose two segments of samples respectively from sensing data of two pre-selected settings (certain PU to SU distances and angles of incidence). For example, group A includes sensing signal sampled when transmitter's antenna points to the receiver's with an angle of $20°$, and the distance between them is fixed at $2m$. Group B includes those sampled when transmitter's antenna points to the receiver's with an angle of $0°$, at the same distance. If we run the MRT based detection algorithm on the data consisting of both groups A and B, we could measure the average delay and false alarm for hypothesis testing H_0 and H_1. Then we adjust the decision rule by trying different values for the two parameters β and ϵ as mentioned in Procedure 5, and repeat the experiment above, until we obtain the receiver operating characteristic (ROC) curve.

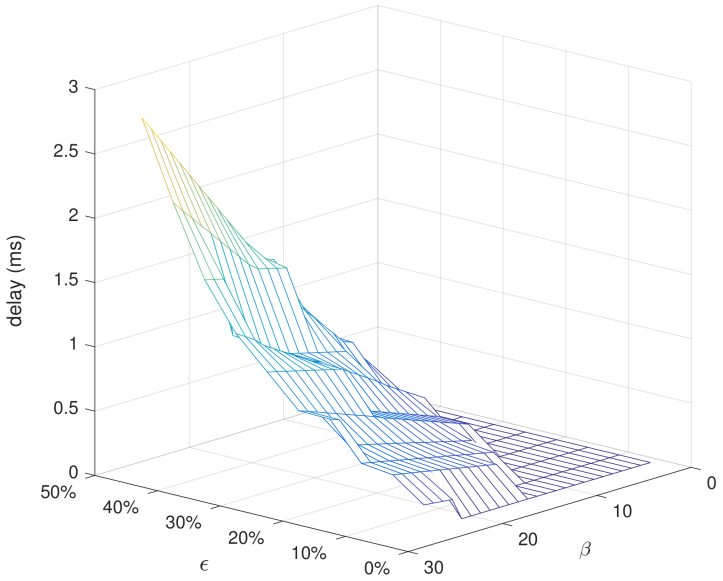

Figure 4.7: Impact of different parameters β and ϵ on detection delay

Each pre-selected setting, namely the distance and angle of incidence before and after the change, corresponds to one ROC curve, because essentially it is related to the difference between the pre-change and post-change statistics. If we assume that X and Y are each subject to a certain distribution, and the random variables are i.i.d., this difference can be measured by the Kullback-Leibler distance. Intuitively, the larger the difference is, the better the detection performance will be, thus making the ROC curve closer to the origin. Fig. 4.7 shows the delay with different values of β and ϵ. As we can see, when the threshold controlled by β increases, the delay increases as well; when the sensitivity fraction ϵ increases, the delay also increases. When β and/or ϵ are too small, the delay tends to 0, which in fact indicates almost sure false alarms.

Fig. 4.8 shows the ROC curve for the setting when the distance between the PU and SU is fixed at $2m$ and the angle of incidence changes from 20° to 0°. The quantization step is set to $P = 20$ and reference sample size is $K = 4000$. Like most detections, we have to find a tradeoff between the false alarm rate and detection delay. We did not take into account the missed detection, when the interval between the status change of the PU is too short for the SU to detect, since we only focus on the sensing from H_0 to H_1 or otherwise.

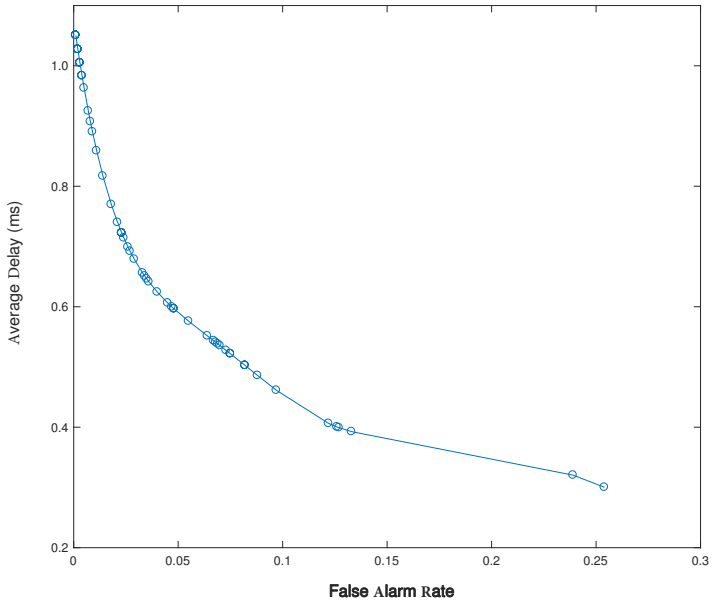

Figure 4.8: ROC: average delay vs. false alarm rate

4.5 Qualitative Performance Analysis

In this section, we will provide some performance analysis on our proposed MRT detection based spectrum sensing. The motivation for us to adopt the MRT detection is: first, simple thresholding does not work well in change point detection, since it will take a random spike as an indicator of hitting a threshold; second, the commonly used likelihood ratio test does not work in our situation, since no certain distributions for pre-change and post-change random processes are assumed; third, in the scenario of mmWave communications, interference is notably mitigated thanks to the directional antenna. Therefore the spectrum sensing only needs to focus on significant changes instead of temporary fluctuations.

The MRT detection essentially utilizes the stationarity of the Markov process. If there is no change, the random process should remain stationary, with the transition matrix unchanged. Therefore the MRT defined in Eq (4.4) for each state should be theoretically unchanged. Once the change occurs, indicating the PU's activities either from absence to presence or vice versa, at least a fraction of the states will have substantially different MRTs. Hence, by setting a threshold parameter β and the fraction ϵ, the SU could detect the change

when the following inequality is satisfied, as we mentioned in previous sections:

$$\frac{1}{P}\sum_{i=1}^{P} 1_{\tau_i \geq E[T_i]+\beta\sqrt{Var[T_i]}} > \epsilon$$

However, there is a limitation of this approach, that the minimum detection delay exists, and it is bounded from below by the minimum MRT of all states plus the deviation, given by

$$D_{min} \geq \min_i \left\{ E[T_i] + \beta\sqrt{Var[T_i]} \right\} \tag{4.7}$$

We can see that it is not only related to β and ϵ but also to the sample mean $E[T_i]$ and variance $Var[T_i]$ of the MRT for each state. Hence, the performance relies on the reference sample size as well. In our experiment, the setup of $P = 20$ and $K = 4000$ will lead to better ROC performance due to the lower error rate for estimation of MRT.

The last but not the least, this MRT detection can also serve as a framework for universal change detection, not only for the change in amplitude but also in other statistics such as phase or frequency. It can be quite useful when no prior knowledge of the pre-change or post-change distribution is given and the sample independency is not guaranteed, as long as the process is stationary Markov process before and after the change point.

4.6 Conclusion

In this chapter we have proposed a universal spectrum sensing technique that can be applied to mmWave cognitive network, where the signal received by SU is vulnerable to environmental interference and thus fluctuates. By quantizing the sensed signal to states in a Markov process, monitoring significant changes in MRT for each state, an SU can know whether the PU is present or not, to decide whether it can use the PU-licensed band to transmit. It provides a way to detect a change in statistics from H_0 to H_1, while not knowing the exact distributions of them. It does not rely on the sample independency, thus being universal. We can also extend this as a detection framework for other areas beyond spectrum sensing.

Chapter 5

Conclusion

This thesis extends the scope of quickest change detection to two practical use cases: multi-agent coorperative detection in networks and universal data-driven quickest detection, and applies proposed quickest detection algorithms to wireless spectrum sensing in cognitive radio, which has been a thoroughly studied topic in regards to spectrum crowdedness problem.

The first chapter describes the limitation of CUSUM quickest detection and necessity of the proposed approaches to make it more applicable to spectrum sensing scenario. Then chapter 2 shows how quickest detection can be used to facilitate dynamic primary user activities detection in coorperative spectrum sensing given non-perfect message passing channel. The finite length approximation of CUSUM with BP in a Gaussian Markov random field has been theoretically analyzed, and the numerically results show the performance gain over BP without change detection scheme.

Then in chapter 3, non-parametric quickest detection algorithm is proposed, which is illuminated by and based on a machine learning based sequential detection algorithm KLIEP and the multi-thread form of optimal CUSUM stopping time. The merit of this universal quickest detection algorithm is that the detection of abrupt change in spectrum occupancy can be carried out without any prior knowledge of pre-change and post-change distribution, which comes with a tradeoff between the increased computational cost and better sensing performance.

Last but not the least, in chapter 4 for spectrum sensing application in mmWave environment, where assumption of i.i.d. random variable does not necessarily hold, a pure data-driven detection framework is proposed based on mean recurrence time of a Markov process. It provides a way to detect a change in statistics from H_0 to H_1, while not knowing the exact distributions of them and also does not rely on the sample independency, thus being truly universal. This framework can also extend to other areas beyond spectrum sensing.

Bibliography

[1] Baykas, T., Sum, C.-S., Lan, Z., Wang, J., Rahman, M. A., Harada, H., and Kato, S. (2011). Ieee 802.15. 3c: the first ieee wireless standard for data rates over 1 gb/s. *IEEE Communications Magazine*, 49(7). 59

[2] Bouman, C. A., Sauer, K., and Saquib, S. (1995). Markov random fields and stochastic image models. In *1995 IEEE International Conference on Image Processing*. 9

[3] Frey, B. J., Brendan, J. F., and Frey, B. J. (1998). *Graphical models for machine learning and digital communication*. MIT press. 7

[4] Ganesan, G. and Li, Y. (2007a). Cooperative spectrum sensing in cognitive radio, part i: Two user networks. *IEEE Transactions on wireless communications*, 6(6):2204–2213. 6

[5] Ganesan, G. and Li, Y. (2007b). Cooperative spectrum sensing in cognitive radio, part ii: multiuser networks. *IEEE Transactions on wireless communications*, 6(6):2214–2222. 6

[6] Ghasemi, A. and Sousa, E. S. (2005). Collaborative spectrum sensing for opportunistic access in fading environments. In *New Frontiers in Dynamic Spectrum Access Networks, 2005. DySPAN 2005. 2005 First IEEE International Symposium on*, pages 131–136. IEEE. 6

[7] Group, X. W. et al. (2006). The xg vision: Rfc. 5

[8] Gustafsson, F. (1996). The marginalized likelihood ratio test for detecting abrupt changes. *IEEE Transactions on automatic control*, 41(1):66–78. 41

[9] Härdle, W. K., Müller, M., Sperlich, S., and Werwatz, A. (2012). *Nonparametric and semiparametric models*. Springer Science & Business Media. 41

[10] Kailath, T. and Poor, H. V. (1998). Detection of stochastic processes. *IEEE Transactions on Information Theory*, 44(6):2230–2231. 28, 51

[11] Kawahara, Y. and Sugiyama, M. (2009). Change-point detection in time-series data by direct density-ratio estimation. In *Proceedings of the 2009 SIAM International Conference on Data Mining*, pages 389–400. SIAM. 47

[12] Koller, D., Friedman, N., and Bach, F. (2009). *Probabilistic graphical models: principles and techniques*. MIT press. 7

[13] Lai, L., Fan, Y., and Poor, H. V. (2008). Quickest detection in cognitive radio: A sequential change detection framework. In *Global Telecommunications Conference, 2008. IEEE GLOBECOM 2008. IEEE*, pages 1–5. IEEE. 40, 41

[14] Lai, T. L. (1998). Information bounds and quick detection of parameter changes in stochastic systems. *IEEE Transactions on Information Theory*, 44(7):2917–2929. 51, 52

[15] Li, C., Li, H., and Dai, H. (2008a). Collaborative quickest detection in adhoc networks with delay constraint-part ii: Multi-node network. In *Information Sciences and Systems, 2008. CISS 2008. 42nd Annual Conference on*, pages 600–605. IEEE. 28, 30

[16] Li, H. (2010a). Cooperative spectrum sensing via belief propagation in spectrum-heterogeneous cognitive radio systems. In *Wireless Communications and Networking Conference (WCNC), 2010 IEEE*, pages 1–6. IEEE. 7, 8, 10, 11, 14

[17] Li, H. (2010b). Reconstructing spectrum occupancies for wideband cognitive radio networks: A matrix completion via belief propagation. In *Communications (ICC), 2010 IEEE International Conference on*, pages 1–6. IEEE. 7, 10

[18] Li, H., Li, C., and Dai, H. (2008b). Quickest spectrum sensing in cognitive radio. In *Information Sciences and Systems, 2008. CISS 2008. 42nd Annual Conference on*, pages 203–208. IEEE. 7, 40, 41

[19] Li, H. and Qian, L. (2011). Cross-network spectrum sensing for mission-critical cognitive radio networks: Collaboration through gateways. In *MILITARY COMMUNICATIONS CONFERENCE, 2011-MILCOM 2011*, pages 1041–1046. IEEE. 7

[20] Lorden, G. et al. (1971a). Procedures for reacting to a change in distribution. *The Annals of Mathematical Statistics*, 42(6):1897–1908. 7, 16, 40, 43

[21] Lorden, G. et al. (1971b). Procedures for reacting to a change in distribution. *The Annals of Mathematical Statistics*, 42(6):1897–1908. 86

[22] MacCartney, G. R., Zhang, J., Nie, S., and Rappaport, T. S. (2013). Path loss models for 5g millimeter wave propagation channels in urban microcells. In *Globecom*, pages 3948–3953. 59

[23] Mishra, S. M., Sahai, A., and Brodersen, R. W. (2006). Cooperative sensing among cognitive radios. In *Communications, 2006. ICC'06. IEEE International conference on*, volume 4, pages 1658–1663. IEEE. 6

[24] Moustakides, G. V. et al. (1986). Optimal stopping times for detecting changes in distributions. *The Annals of Statistics*, 14(4):1379–1387. 16, 27, 28, 51

[25] Murphy, K. P., Weiss, Y., and Jordan, M. I. (1999). Loopy belief propagation for approximate inference: An empirical study. In *Proceedings of the Fifteenth conference on Uncertainty in artificial intelligence*, pages 467–475. Morgan Kaufmann Publishers Inc. 26

[26] North, R. (2006). Joint tactical radio system: Connecting the gig to the tactical edge. In *MILCOM(MILCOM)*, volume 00, pages 1–6. 5

[27] Oskiper, T. and Poor, H. V. (2005). Quickest detection of a random signal in background noise using a sensor array. *EURASIP Journal on Applied Signal Processing*, 2005:13–24. 7

[28] Page, E. S. (1954). Continuous inspection schemes. *Biometrika*, 41(1/2):100–115. 27, 41, 50, 65

[29] Pearl, J. (1986). Fusion, propagation, and structuring in belief networks. *Artificial intelligence*, 29(3):241–288. 20

[30] Perahia, E., Cordeiro, C., Park, M., and Yang, L. L. (2010). Ieee 802.11 ad: Defining the next generation multi-gbps wi-fi. In *Consumer Communications and Networking Conference (CCNC), 2010 7th IEEE*, pages 1–5. IEEE. 59

[31] Pi, Z. and Khan, F. (2011). An introduction to millimeter-wave mobile broadband systems. *IEEE communications magazine*, 49(6). 59

[32] Poor, H. V. and Hadjiliadis, O. (2009). *Quickest detection*, volume 40. Cambridge University Press Cambridge. 1, 7, 27, 31, 40

[33] Pyke, R. (1961). Markov renewal processes: definitions and preliminary properties. *The Annals of Mathematical Statistics*, pages 1231–1242. 61

[34] Rogers, L. C. G. and Williams, D. (2000). *Diffusions, Markov processes and martingales: Volume 2, Itô calculus*, volume 2. Cambridge university press. 27

[35] Senadji, B. and Chang, K. (2013). Detection of dynamic primary user with cooperative spectrum sensing. In *2013 Proceedings of the 21st European Signal Processing Conference (EUSIPCO)*, pages 1–5. IEEE. 10

[36] Sugiyama, M., Suzuki, T., Nakajima, S., Kashima, H., von Bünau, P., and Kawanabe, M. (2008). Direct importance estimation for covariate shift adaptation. *Annals of the Institute of Statistical Mathematics*, 60(4):699–746. 41, 46, 47, 48

[37] Taylor, H. M. (1975). A stopped brownian motion formula. *The Annals of Probability*, pages 234–246. 27

[38] Tomkins, A., Aroca, R. A., Yamamoto, T., Nicolson, S. T., Doi, Y., and Voinigescu, S. P. (2009). A zero-if 60 ghz 65 nm cmos transceiver with direct bpsk modulation demonstrating up to 6 gb/s data rates over a 2 m wireless link. *IEEE journal of solid-state circuits*, 44(8):2085–2099. 61

[39] Unnikrishnan, J. and Veeravalli, V. V. (2008). Cooperative sensing for primary detection in cognitive radio. *IEEE Journal of selected topics in signal processing*, 2(1):18–27. 6, 9

[40] Unnikrishnan, J., Veeravalli, V. V., and Meyn, S. P. (2011). Minimax robust quickest change detection. *IEEE Transactions on Information Theory*, 57(3):1604–1614. 41

[41] Wald, A. (1947). Sequential analysis. 30, 86

[42] Wang, Q., Kulkarni, S. R., and Verdú, S. (2006). A nearest-neighbor approach to estimating divergence between continuous random vectors. In *Information Theory, 2006 IEEE International Symposium on*, pages 242–246. IEEE. 41, 45, 48

[43] Wang, Y. and Li, H. (2016). Universal quickest spectrum sensing. In *Global Communications Conference (GLOBECOM), 2016 IEEE*, pages 1–6. IEEE. 65

[44] Weiss, Y. and Freeman, W. T. (2000). Correctness of belief propagation in gaussian graphical models of arbitrary topology. In *Advances in neural information processing systems*, pages 673–679. 14, 20

[45] Xiao, S.-Q. and Zhou, M.-T. (2008). *Millimeter wave technology in wireless PAN, LAN, and MAN*. CRC Press. 59

[46] Yedidia, J. S., Freeman, W. T., and Weiss, Y. (2003). Understanding belief propagation and its generalizations. *Exploring artificial intelligence in the new millennium*, 8:236–239. 7

[47] Zarrin, S. and Lim, T. J. (2008). Belief propagation on factor graphs for cooperative spectrum sensing in cognitive radio. In *New Frontiers in Dynamic Spectrum Access Networks, 2008. DySPAN 2008. 3rd IEEE Symposium on*, pages 1–9. IEEE. 7, 10

[48] Zhang, Z., Bao, J., Fan, Y., and Li, H. (2018). Tracking via blocking in millimeter wave communication networks. In *2018 IEEE International Conference on Communications (ICC)*, pages 1–6. 59

[49] Zhang, Z., Li, L., Fan, Y., and Li, H. (2018). Object tracking via blocking in millimeter wave communications: A blessing misfortune. In *2018 IEEE International Conference on Communications (ICC)*, pages 1–6. IEEE. 59

Appendices

A Proof of Lemma 2.1

Proof. By the nature of matrix Q as in (2.24) we can relate V_{xy} and $\boldsymbol{y}$ to the ones in the unwrapped tree. For convenience, we copy (2.24) and (2.25) here as follows:

$$\hat{\boldsymbol{y}} = Q\boldsymbol{y}, \tag{1}$$

$$\hat{V}_{xy}Q = QV_{xy}, \tag{2}$$

$$\hat{V}_{xx}Q + \Delta = QV_{xx} \tag{3}$$

By marginalization, we can obtain the conditional mean of $\hat{x}$ given the observation $\hat{y}$ as in Eq. (2.22). For the graph $\hat{G}'$, we have

$$\hat{V}_{xx}\hat{\mu} = -\hat{V}_{xy}\hat{\boldsymbol{y}} \tag{4}$$

Based on equations from (1) to (4), we can easily obtain

$$\hat{V}_{xx}\hat{\mu} = -QV_{xy}\boldsymbol{y} \tag{5}$$

For the true expectation of loopy network, we have

$$V_{xx}\mu = -V_{xy}\boldsymbol{y} \tag{6}$$

We multiply (6) by Q, and multiply (3) by μ. Combining these two, we then have

$$\hat{V}_{xx}Q\mu + \Delta\mu = QV_{xx}\mu = -QV_{xy}\boldsymbol{y} \tag{7}$$

From (5) and (7), we have

$$\hat{V}_{xx}Q\mu + \Delta\mu = \hat{V}_{xx}\hat{\mu} \tag{8}$$

Since the covariance matrix for unwrapped tree $\hat{C}_{\boldsymbol{x}|\boldsymbol{y}} = \hat{V}_{xx}^{-1}$, we left multiply (8) by $\hat{C}_{\boldsymbol{x}|\boldsymbol{y}}$, thus resulting in

$$Q\mu + \hat{C}_{\boldsymbol{x}|\boldsymbol{y}}\Delta\mu = \hat{\mu} \tag{9}$$

By taking the first row on both sides of (9), Eq, (2.26) is thus proved. □

B Proof of Lemma 2.2

Proof. From $V_{xx}^{-1} = C_{x|y}$, we know

$$V_{xx}C_{x|y} = I \tag{10}$$

Therefore,

$$V_{xx}C_{x_1|y}^T = (1\ 0\ 0\ 0\ 0\cdots 0)^T \tag{11}$$

Denote by e_1 the vector $(1\ 0\ 0\ 0\ 0\cdots 0)^T$. By (3) and (11) we have

$$\hat{V}_{xx}QC_{x_1|y}^T + \Delta C_{x_1|y}^T = Qe_1 \tag{12}$$

Similarly to (11), we can obtain

$$\hat{V}_{xx}\hat{C}_{x_1|y}^T = (1\ 0\ 0\ 0\ 0\cdots 0)^T = \hat{e}_1 \tag{13}$$

Subtracting (12) from (13) yields

$$\hat{C}_{x_1|y} = QC_{x_1|y}^T + \hat{C}_{x|y}\Delta C_{x_1|y}^T + \hat{C}_{x|y}(\hat{e}_1 - Qe_1) \tag{14}$$

Take the first row on both sides, we have

$$\hat{\sigma}^2(1) = \sigma^2(1) + \hat{C}_{x_1|y}\Delta C_{x_1|y}^T + \hat{C}_{x_1|y}(\hat{e}_1 - Qe_1) \tag{15}$$

□

C Proof of Lemma 2.4

Proof. Since we need to guarantee the same message flows in the original graph G and the unwrapped tree $\hat{G}$, we can first construct an unwrapped tree $\hat{G}$, with any desired depth m. Then we modify the local function $\psi_i(\hat{x}_i|\hat{y}_i)$ and the observations in the leaves as follows:

- for each leaf node $\hat{x}_i$ (which corresponds to $x_{i'}$ in the cyclic graph G), set $\psi_i(\hat{x}_i|\hat{y}_i)$ and $\hat{y}_i$ such that the message sent from $\hat{y}_i$ to $\hat{x}_i$ is the product of belief messages (under fixed point ϕ) sent from the neighbors of $x_{i'}$ excluding the parent node of $\hat{x}_i$.

- for any two adjacent nodes $\hat{x}_i,\ \hat{x}_j$ in $\hat{G}$, if both of them are replicas from the same node $x_{i'}$ in G, one will forward any message it receives to the other without any calculation.

By this construction, all the leaves in $\hat{G}$ will send messages to their neighbors based on the fixed point ϕ. All non-leaf nodes in $\hat{G}$ have the same relationship with their neighbors as the corresponding nodes in G, except for the buffer nodes, which will not affect the message passing algorithm. The local message passing updates are the same as those in G. □

D Proof of Theorem 2.5

Proof. We denote by $\hat{\mu}$ the conditional expectation in modified $\hat{G}$. By the result of Lemma 2.4, we have

$$\hat{\mu} = Q\mu_0 \tag{16}$$

where μ_0 is the posterior expectation under the fixed point ϕ. We know that $\hat{\mu}$ is a solution to (4). Therefore by substituting (16) into (4) we have

$$\hat{V}_{xx}Q\mu_0 = -\hat{V}_{xy}\hat{\boldsymbol{y}} \tag{17}$$

Denote by $[\cdot]_k$ the first k rows of a matrix or column vector. Applying this operator on (17), we have

$$[\hat{V}_{xx}Q]_k\mu_0 = -[\hat{V}_{xy}\hat{\boldsymbol{y}}]_k \tag{18}$$

Similarly for $k < M - l$, we have

$$[\hat{V}_{xx}Q]_k = [QV_{xx}]_k, \quad [\hat{V}_{xy}\hat{\boldsymbol{y}}]_k = [QV_{xy}\boldsymbol{y}]_k \tag{19}$$

Combining (18) and (19) gives

$$[Q]_k V_{xx}\mu_0 = -[Q]_k V_{xy} y, \ \forall\ k < M - l \tag{20}$$

Since we can expand the unwrapped tree to any depth, we can always find a sufficiently large M to make (21) hold. Thus the expectations derived from ϕ are exact:

$$V_{xx}\mu_0 = -V_{xy} y, \tag{21}$$

□

E Proof of Theorem 2.6

Proof. By the extended Wald's Identity and the inequality (A.205) in [41] we show that

$$\begin{aligned} &I_A E_1[T_A] + I_B E_1[\max(T_A - D, 0)] \\ \geq &(1-\beta_0) log\left(\frac{1-\beta_0}{\alpha_0}\right) + \beta_0 log\left(\frac{\beta_0}{1-\alpha_0}\right) + DI_B \end{aligned} \tag{22}$$

where α_0 and β_0 are the error probabilities of one-sided sequential test. Then we use the same procedure as that of Eq. (15) in [21] to prove the following fact: for any $\epsilon \in (0,1)$ and any stopping time T_A, $\exists C(\epsilon) < \infty$ such that

$$I_A E_1[T_A] + I_B E_1[\max(T_A - D, 0)] \geq (1-\epsilon)\log E_\infty[T_A] - C(\epsilon). \tag{23}$$

Then, based on Brownian motion approximation and (23), we can obtain

$$I_A \mathcal{D}_A + I_B \max(\mathcal{D}_A - D, 0) \geq \log \mathcal{F}_A \ \ as\ \gamma_A \to \infty \tag{24}$$

Also we have the inequality in the opposite direction based on (2.47) and (2.50)

$$I_A \mathcal{D}_A + I_B \max(\mathcal{D}_A - D, 0) \leq \log \mathcal{F}_A \ \ as\ \gamma_A \to \infty \tag{25}$$

Therefore the equality holds asymptotically. □

F Definition of MRT

Consider a discrete time Markov chain with the transition probability p_{ij}^n, where p_{ij}^n means the probability that the state transits from i to j after exact n steps. Then, the mean recurrent time of state i is defined as

$$MRT_i = \sum_{n=1}^{\infty} np_{ii}^n. \tag{26}$$

If MRT_i is finite, state i is called positive recurrent. Note that the state i is called recurrent, if its probability of finite return time is 1, which is weaker than the finite mean return time.

Vita

Yifan Wang was born in Ya'an, P.R. China. He received his Bachelor of Engineering degree in communication engineering from University of Electronic Science and Technology of China in 2010. He started his graduate study at The University of Tennessee, Knoxville, in August 2012. His research interests include statistic signal processing, smart grid communication, sequential detection, wireless communication network, etc. From May to September 2016, he worked as a student intern in Climate Change Sciences Institute, Oak Ridge National Lab. After working for half a year as data scientist in Resonova International Consulting, he joined Argo AI as software engineer in January 2019 and has since been working in Argo's system team on performance analysis of autonomous vehicle. He will obtain his Doctor of Philosophy degree in Electronic and Electrical Engineering in August 2019.